Cancer chess: molecular insights into PARP inhibitor resistance

Barazas, M.

Abstract

Selective elimination of BRCA1-deficient cells by inhibitors of poly(ADP-ribose) polymerase (PARP) is a prime example of the concept of synthetic lethality in cancer therapy. This interaction is counteracted by the restoration of BRCA1-independent homologous recombination through loss of factors such as 53BP1, RIF1, and REV7/MAD2L2, which inhibit end resection of DNA double-strand breaks (DSBs). To identify additional factors involved in this process, we performed CRISPR/SpCas9-based loss-of-function screens and selected for factors that confer PARP inhibitor (PARPi) resistance in BRCA1-deficient cells. Loss of members of the CTC1-STN1-TEN1 (CST) complex were found to cause PARPi resistance in BRCA1-deficient cells *in vitro* and *in vivo*. We show that CTC1 depletion results in the restoration of end resection and that the CST complex may act downstream of 53BP1/RIF1. These data suggest that, in addition to its role in protecting telomeres, the CST complex also contributes to protecting DSBs from end resection.

Cancer Chess: Molecular Insights Into PARPi Resistance

The CST Complex Mediates End Protection at Double-Strand Breaks and Promotes PARP Inhibitor Sensitivity in BRCA1-Deficient Cells

Chapter 6

Adapted from:
***Marco Barazas**, Stefano Annunziato, Stephen J Pettitt, Inge de Krijger, Hind Ghezraoui , et al.*
Cell Reports. 2018; 23(7): 2107-2118.

Introduction

The synthetic lethal interaction between BRCA1 deficiency and poly(ADP-ribose) polymerase (PARP) inhibition is a well-established therapeutic paradigm with encouraging response rates in the clinic [1]. This has resulted in the recent regulatory approval of three PARP inhibitors (PARPis) for the treatment of serous ovarian cancers and one PARPi, olaparib, for the treatment of *BRCA*-mutated, HER2-negative breast cancers. Moreover, the BRCA-PARP paradigm might be extended beyond breast and ovarian cancer because recent clinical studies indicate that a subset of prostate cancers harbor a homologous recombination (HR) defect and, hence, might benefit from olaparib treatment [2, 3].

Despite this success, long-lasting clinical response rates in patients with advanced disease are limited by the development of resistance, the mechanisms of which have not been fully elucidated. A major class of resistance mechanisms centers on re-expression of functional BRCA1 or BRCA2 protein, either through promoter demethylation, genetic reversion, or gene fusions [4-6]. However, our previous work also identified the existence of additional BRCA1-independent resistance mechanisms in the *K14cre;Brca1*$^{F/F}$*; p53*$^{F/F}$ (KB1P) genetically engineered mouse model of hereditary breast cancer [7]. In this model, re-expression of functional BRCA1 is excluded because of the large, engineered, intragenic *Brca1* deletion, which spans multiple exons. Despite the absence of functional BRCA1 restoration, KB1P tumors acquired resistance to PARPi treatment. In addition to activation of the P-glycoprotein drug efflux transporter [8], the BRCA1-independent resistance mechanisms in KB1P tumors predominantly involved the partial restoration of HR activity through re-wiring of the DNA damage response (DDR); for example, by loss of 53BP1 [9-11]. These seminal findings have spurred a number of studies in which additional downstream antagonists of end resection were identified, including RIF1 [12-15] and REV7/MAD2L2 [16, 17]. However, the currently known resistance factors cannot explain all PARPi-resistant cases, suggesting that additional proteins functioning in this pathway remain to be identified. Moreover, although the loss of resection antagonists partially restores end resection of DNA double-strand breaks (DSBs), none of these factors have direct functions in DNA metabolism, raising the question of how DNA metabolism at DSBs might be altered to stimulate end resection.

The function of the 53BP1 pathway is not exclusive to canonical DSB repair, but it also acts on telomeres [18]. Because telomere ends resemble DSBs located at chromosomal termini, cells have evolved several mechanisms to protect telomeres from DSB end processing and chromosome end-to-end fusions [19]. Mammalian telomeres consist of TTTAGG repeats ending with a single-strand G-rich overhang. The single-stranded DNA (ssDNA) overhang is crucial in telomere maintenance because it is required for the formation of the T-loop structure [20, 21]. Notably, excessive resection of telomere ends is inhibited by the action of the shelterin complex and by the 53BP1 pathway [19, 22].

Besides the mechanisms that have evolved to protect telomeric overhangs from excessive processing, it has recently been shown that the RPA-like CTC1-STN1-TEN1 (CST) complex is able to localize to telomeric ssDNA and mediate a fill-in reaction executed by polymerase-alpha (POLA) to buffer resection activity [23-25]. Notably, it was demonstrated that the binding of the CST complex to ssDNA is not particularly sequence-specific, although a partial preference for G-rich regions has been described [24, 26]. Additionally, CST components do not localize exclusively to telomeres [24]. This might argue that the CST complex also has non-telomeric functions.

In this study, three independent forward genetic CRISPR/SpCas9-based loss-of-function screening approaches were employed to identify factors that induce PARPi resistance in BRCA1-deficient cells. Together, these screens identified that defects in *Ctc1*, or its CST complex members *Stn1* or *Ten1*, suppress the synthetic lethal interaction between BRCA1 and PARP inhibition. Inactivation of CTC1 is sufficient to drive PARPi resistance *in vivo*. Depletion of CTC1 increased end resection activity and subsequently restored RAD51 focus formation upon ionizing radiation (IR)-induced DNA damage, providing a mechanistic basis for these observations. Moreover, the CST complex facilitates canonical non-homologous end joining (c-NHEJ)-driven repair. Together, these data demonstrate that the CST complex plays a more global role in DNA repair beyond the protection of telomeres.

Results

Forward Genetic CRISPR/SpCas9 Screens Identify Selective Enrichment for Loss of CTC1 during PARPi Treatment in BRCA1-Deficient Cells

To identify factors that modulate the synthetic lethal interaction between BRCA1 and PARP, we carried out three independent forward genetic loss-of-function CRISPR/SpCas9 screens (Fig. 1). All screens were analyzed by harvesting cells before and after PARPi treatment, after which single guide RNA (sgRNA) sequences were amplified from genomic DNA by PCR and analyzed by next-generation sequencing. The screening data were processed by the model-based analysis of genome-wide CRISPR-Cas9 knockout (MAGeCK) or the drugZ algorithm [27, 28], and the results were sorted on positive selected gene ranks to allow comparison across screens. Additional experimental details are provided in the Supplementary Materials and Methods.

The first PARPi resistance screen was performed in SpCas9-expressing KB1P-G3 mouse mammary tumor cells [11] using a custom-made lentiviral sgRNA library targeting 1,752 DDR-related genes (Table S1) cloned into the doxycycline-inducible pLenti-sgRNA-tetR-T2A-PuroR vector [29]. The screen was performed at 100× coverage, and cells were selected with two different PARPis, olaparib and AZD2461 [30], at the approximate inhibitory concentration 90 (IC90) for 14 days (Fig. 1A). Although sgRNAs targeting *Tp53bp1* were deliberately removed from the library to avoid the possibility

that this potent PARPi resistance factor might obscure the effects of other genes, its upstream regulatory factor *Rnf8* scored among the top genes (Fig. 1B).

The second PARPi resistance screen was performed in SpCas9-expressing *Brca1*$^{-/-}$*;Trp53*$^{-/-}$ mouse embryonic stem cells (mESCs) infected with a genome-wide lentiviral sgRNA library targeting 19,150 genes [31]. The screen was performed at 75× coverage in two independent transductions, and cells were selected with olaparib at a concentration of 15 nM for 10 days. As expected, *Tp53bp1* and *Rnf8* scored among the top genes and ranked #1 and #15, respectively (Fig. 1C).

A third PARPi resistance screen was performed in *BRCA1*^{2288delT} mutant SUM149PT human breast cancer cells [32]. SUM149PT cells expressing doxycycline-inducible SpCas9 were lentivirally infected with a genome-wide sgRNA library targeting 18,010 genes [33]. This screen was performed at 1,000× coverage, and cells were selected in the presence of doxycycline plus 100 nM talazoparib for 2 weeks. The screen was dominated by sgRNAs targeting *PARP1*, the drug target of talazoparib. Although PARP1 loss is expected to be lethal in BRCA1-deficient cells, the selection for PARP1 loss in SUM149PT cells might be attributed to residual BRCA1 activity, which might enable cell survival in the absence of PARP [34, 35]. Moreover, *TP53BP1* scored among the top enriched genes and ranked #7 (Fig. 1D).

The results from these three independent screens were collated to identify consistent outliers. The top 20 genes were selected from the DDR-focused library screen in KB1P-G3 cells. Because the genome-wide libraries contain about 10-fold more genes than the DDR-focused library, the top 200 genes were selected from the mESC and SUM149PT screens, and these were plotted in a Venn diagram (Fig. 1E). Notably, *Ctc1* was the only gene that consistently scored in all three screens (ranked #10, #39, and #39 in the KB1P-G3, mESC, and SUM149PT screens, respectively). Moreover, *Stn1* (also known as *Obfc1*) scored in two of three screens. These results caught our attention because both CTC1 and STN1 are members of the CST complex. Although the CST complex has known functions in telomere metabolism, these PARPi resistance screens might point toward non-telomeric functions of the CST complex. Because *Ctc1* was a top hit in all three independent screens in both mouse and human cells, we prioritized this gene for further validation.

Depletion of CTC1 Suppresses the Synthetic Lethal Interaction between BRCA1 Deficiency and PARP Inhibition

To validate the effect of CTC1 on PARPi sensitivity in BRCA1-deficient cells, we transfected KB1P-G3 cells with pX330 vectors containing three sgRNAs targeting a putative oligonucleotide-binding (OB) fold domain of *Ctc1* (Fig. 2A). The polyclonal targeted populations were efficiently modified for the target site (Fig. 2B–D), as shown by TIDE (tracking of insertions or deletions [indels] by decomposition) analysis [36]. These populations were subsequently treated with olaparib (75 nM) or AZD2461

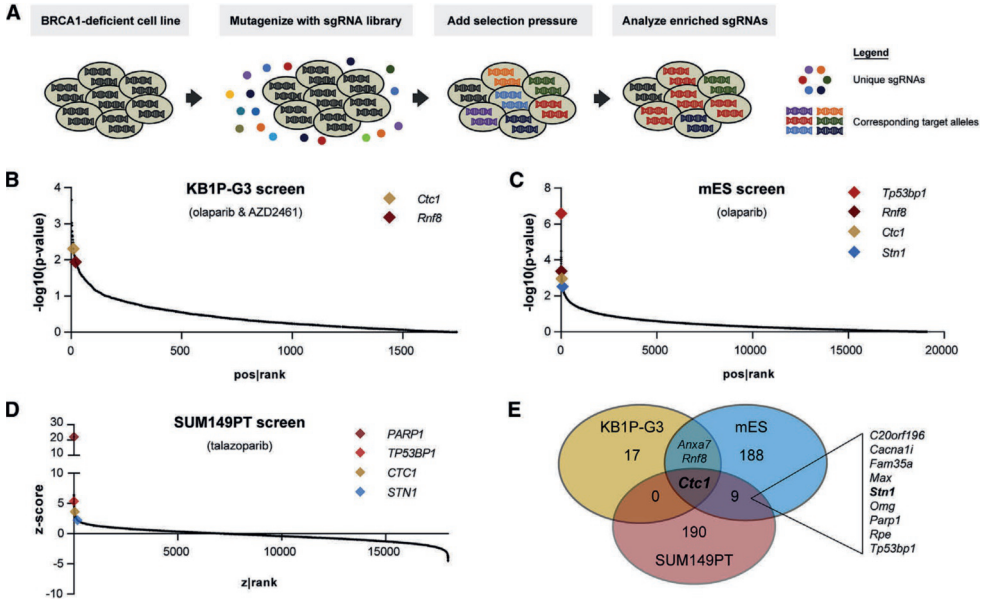

FIGURE 1 | Multiple Independent CRISPR/SpCas9 Loss-of-Function Screens Identify CTC1 as a Driver of PARPi Resistance in BRCA1-Deficient Cells. *(A)* Schematic overview of the screening approach utilized across the different screens. Each screen was performed on a different cell line and screened with a different library, which is indicated per screen. *(B)* SpCas9-expressing KB1P-G3 cells were screened with a DNA damage response (DDR)-focused library at 100× coverage. Cells were plated for clonogenic growth in the presence of olaparib (75 nM) or AZD2461 (250 nM) for 14 days, and sgRNA abundance in treated populations was compared with the starting population using MAGeCK software. Gene-based p values were log-transformed and plotted based on the positive rank (enrichment). Each dot represents a unique gene. *(C)* *Brca1*$^{-/-}$;*Trp53*$^{-/-}$ mouse embryonic stem cells (mESCs) were screened with a genome-wide library in two independent transductions at 75× coverage. After 10 days of culture in the presence of olaparib (15 nM), treated populations were compared with the untreated population using MAGeCK software. Gene based p values were log-transformed and plotted based on the positive rank (enrichment). Each dot represents a unique gene. *(D)* A derivative of the *BRCA1* mutant SUM149PT human triple-negative breast tumor cell line carrying a doxycycline-inducible SpCas9 expression construct was lentivirally infected with a genome-wide guide RNA library at more than 1,000× coverage. Cells were cultured in the presence of doxycycline plus 100 nM talazoparib for 2 weeks. The sgRNA abundance in treated populations was compared with the starting population using drugZ. Gene-based *Z* scores were log-transformed and plotted based on the positive z-rank (enrichment). Each dot represents an individual gene.

(250 nM), the same concentrations as used for the screen. As expected, parental KB1P-G3 cells or KB1P-G3 cells targeted by a non-targeting sgRNA (sgNT) showed high sensitivity to PARPi treatment. In contrast, *Ctc1*-targeted cells showed resistance to treatment, indicating that depletion of CTC1 suppresses the synthetic lethal interaction between BRCA1 deficiency and PARP inhibition (Fig. 2E-F). This could not be attributed to an effect on cell proliferation because we observed no difference in the doubling time upon depletion of CTC1 (Fig. 2G).

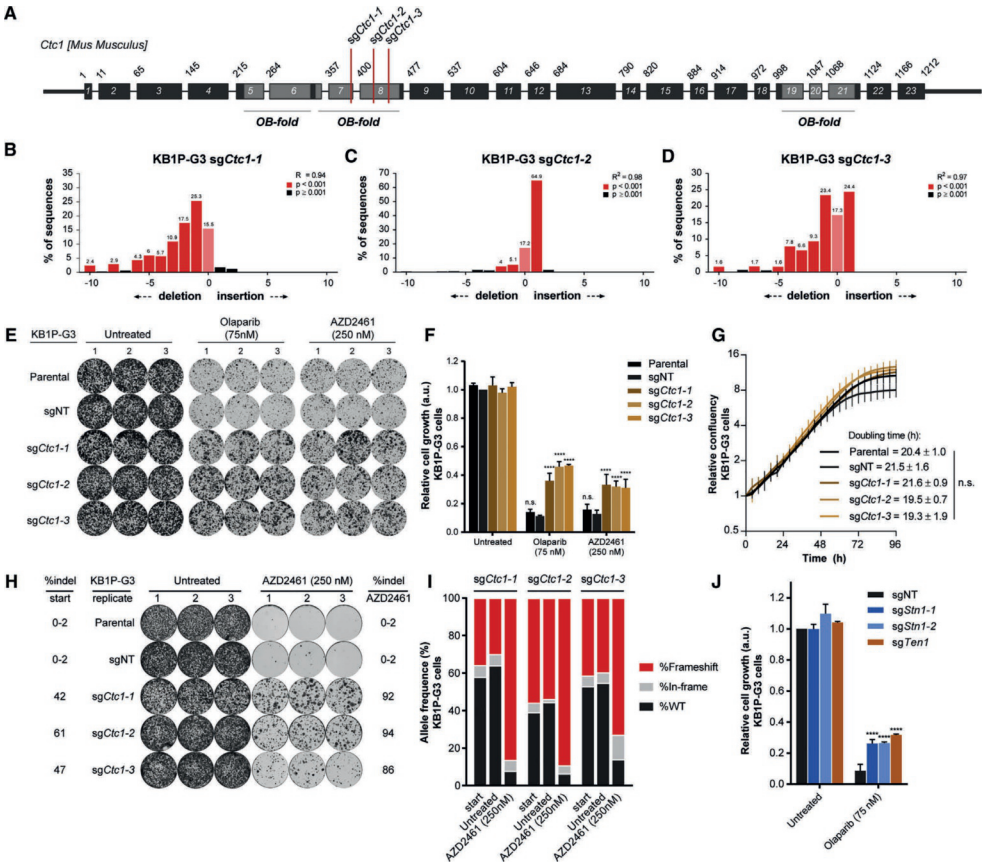

FIGURE 2 | Depletion of CTC1 Suppresses the Synthetic Lethal Interaction between BRCA1 Deficiency and PARP Inhibition. *(A)* Schematic overview of the *Ctc1* gene, in which putative OB fold domains and sgRNA target locations are indicated (adapted from [24]). *(B–D)* KB1P-G3 cells were transfected with pX330puro vectors containing the indicated sgRNAs, and the target region was PCR-amplified to verify allele modification using TIDE software. *(E)* The indicated *Ctc1*-mutated KB1P-G3 cell lines were plated for clonogenic growth upon olaparib (75 nM) or AZD2461 (250 nM) treatment. Three independent experiments were performed, and each condition was plated in triplicate. One representative well per condition is shown for each independent experiment. *(F)* Quantification of crystal violet staining in (E). Data were plotted relative to the growth of untreated sgNT cells and are presented as mean ± SD (n = 3 independent experiments). Significance was calculated by two-way ANOVA with Dunnett's multiple comparisons test (**** adjusted p = 0.0001). *(G)* Relative cell proliferation was determined by IncuCyte Zoom Live – Cell Analysis System measurements. Each data point represents the average of three independent experiments, and in each experiment, six replicate wells were measured and averaged. Data represent mean ± SD (n = 3). Doubling times (exponential growth equation) were calculated using GraphPad software, and significance was calculated by one-way ANOVA with Dunnett's multiple comparisons test. *(H-I)* SpCas9-expressing KB1P-G3 cells were transduced with doxycycline-inducible pLenti-sgRNA-tetR-T2A-PuroR vectors containing the indicated sgRNAs. Polyclonal populations were plated for clonogenic growth with or without AZD2461 (250 nM) *(H)*. Cells were passaged every 10 days for a total of three times. At the endpoint, wells were fixed and stained with crystal violet, and allele distributions were determined from each condition using TIDE software *(I)*. *(J)* KB1P-G3 cells were transfected with pX330puro vectors containing sgRNAs targeting *Stn1* and *Ten1* and cultured in the presence or absence of 75 nM olaparib as in *(E)*. Data were analyzed as in *(F)* and reflect at least two independent experiments.

We next investigated whether *Ctc1*-mutated cells would be specifically selected out from a mixed population by prolonged PARPi treatment. A competition assay was performed in which the evolution of polyclonal populations was monitored by the TIDE algorithm to quantify changes in allele distributions. sgRNAs were cloned in the pLenti-sgRNA-tetR-T2A-Puro vector and introduced in SpCas9-expressing KB1P-G3 cells by lentiviral transduction. The population was mutagenized by doxycycline-induced expression of the sgRNA for 5 days, after which cells were plated without doxycycline for clonogenic growth. After 10 days of culture in the presence or absence of AZD2461, the cells were harvested and re-plated at equal amounts every 10 days for an additional two rounds, resulting in a total treatment duration of 30 days. Although non-transduced cells or cells transduced with a non-targeting sgRNA were effectively killed by this prolonged treatment, *Ctc1*-targeted cells survived (Fig. 2H). This coincided with an enrichment of *Ctc1* frameshift mutations compared with untreated populations, which were kept in culture for the same duration (Fig. 2I).

To study whether this effect is CTC1-specific or a feature of the CST complex, we genetically inactivated the other two CST complex members *Stn1* and *Ten1*, and treated these cells with olaparib under the same conditions as used for *Ctc1*. CRISPR/SpCas9-mediated disruption of *Stn1* or *Ten1* also induced PARPi resistance, recapitulating the effect of *Ctc1* (Fig. 2J). This is consistent with the identification of STN1 in the PARPi resistance screens (Fig. 1E) and shows that PARPi sensitivity is modulated by all CST complex members rather than CTC1 alone.

These data were corroborated in *Brca1*$^{-/-}$*;Trp53*$^{-/-}$ mESCs in which CRISPR/SpCas9-assisted inactivation of *Ctc1* increased survival upon olaparib treatment, which was accompanied by a selection for frameshifting alleles (Supplementary Fig. S1A-B). Furthermore, we targeted the CST complex members in *R26*^{CreERT2}*;Brca1*$^{Sco/\Delta}$ mESCs, which harbor a selectable conditional Brca1^{Sco} allele that can be inactivated by CreERT2 through the addition of 4-hydroxytamoxifen (4-OHT) [9]. Although 4-OHT-induced inactivation of BRCA1 caused lethality in untransduced *R26*^{CreERT2}*;Brca1*$^{Sco/\Delta}$ mESCs, clonal outgrowth was observed for cells depleted of CTC1, STN1, or TEN1 (Fig. 3A). Complete switching of the conditional *Brca1*^{Sco} allele in the surviving population was confirmed by PCR, ruling out that clonal outgrowth was due to a non-recombined *Brca1*^{Sco} allele (Fig. 3B). Finally, depletion of CTC1 in SUM149PT cells enhanced cell survival in the presence of talazoparib, as did depletion of 53BP1 (Fig. 3C), confirming that this effect was not restricted to mouse cells.

In summary, we confirmed that the CST complex promotes PARPi-induced cell lethality in BRCA1-deficient cells. We therefore looked at the role of the CST complex in preventing global DNA damage, focusing on CTC1.

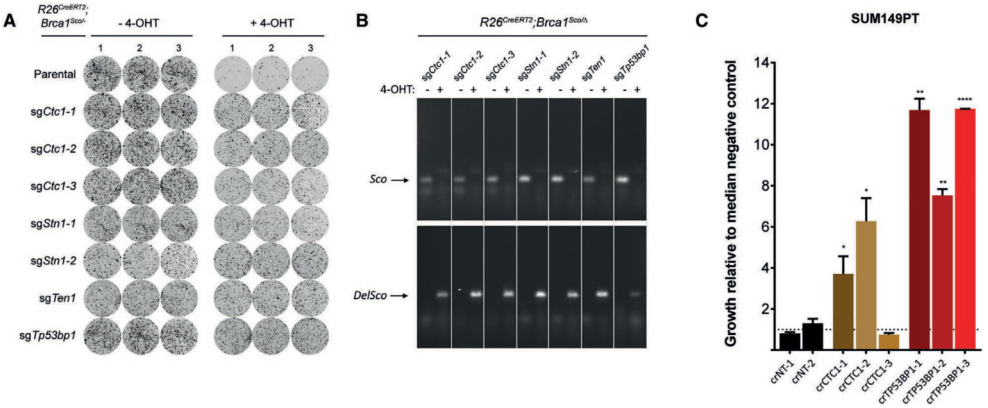

FIGURE 3 | Loss of CST Complex Members Induces PARPi Resistance in BRCA1-Deficient mESCs and SUM149PT Breast Cancer Cells. *(A) Ctc1*, *Stn1*, and *Ten1* were targeted in *R26*^{CreERT2};*Brca1*$^{Sco/\Delta}$ mESCs using pLentiCRISPRv2 vectors. Following transduction and selection, the *Brca1-Sco* allele was recombined by activation of CreERT2 via addition of 4-OHT, after which cells were plated out for clonogenic growth. Cells were fixed and stained with crystal violet. *(B) Brca1* alleles from surviving populations were PCR-amplified using specific primers to detect *Brca1*^{Sco} (*Sco*) and recombined *Brca1*$^{\Delta Sco}$ (*DelSco*) alleles. *(C) BRCA1*-mutant SUM149PT cells were transfected with the EditR CRISPR system, and the indicated CRISPR RNA (crRNA) and then continuously cultured in the presence of 50 nM talazoparib over a 14-day period, at which point cell viability was estimated by use of CellTiter-GLo reagent. Median effects from three independent experiments are shown. Error bars represent SEM. $^{*}p = 0.0415$ and 0.0201, respectively; $^{**}p = 0.0013$ and 0.0011, respectively; $^{****}p = < 0.0001$; unpaired two-tailed Student's t test.

CTC1 Antagonizes End Resection at Non-Telomeric DSBs

During the repair of DSBs, a critical decision is made between initiating repair via NHEJ or via HR, which both require distinct end processing. This decision is tightly balanced by end protection factors, such as 53BP1 or RIF1, which antagonize resection to direct repair via NHEJ, and BRCA1, which promotes end resection to direct repair via HR [12, 14, 18, 23, 37]. It was previously shown that the end resection defect in BRCA1-deficient cells can be rescued via loss of 53BP1, and this also rescued cell lethality induced by BRCA1 loss [9, 38]. Hence, the finding that loss of the CST complex (Fig. 3A) rescued BRCA1 lethality points toward a potential inhibitory role in DSB end resection. Moreover, depletion of CTC1 did not induce PARPi resistance in BRCA2-deficient cells (Supplementary Fig. S2A-B), which is in line with a possible role of the CST complex upstream of BRCA2.

DSB end resection produces ssDNA overhangs, which are protected from nucleolytic degradation and the formation of secondary structures by the coating of RPA. Therefore, we visualized RPA loading in response to α-particle-induced DNA damage by immunofluorescence as a readout for end resection [39]. In line with previous studies [25, 40], KB1P-G3 tumor cells showed a clear resection defect that was partially restored in *Ctc1*-mutated KB1P-G3 cells but not in sgNT-transfected control cells (Fig. 4A-B).

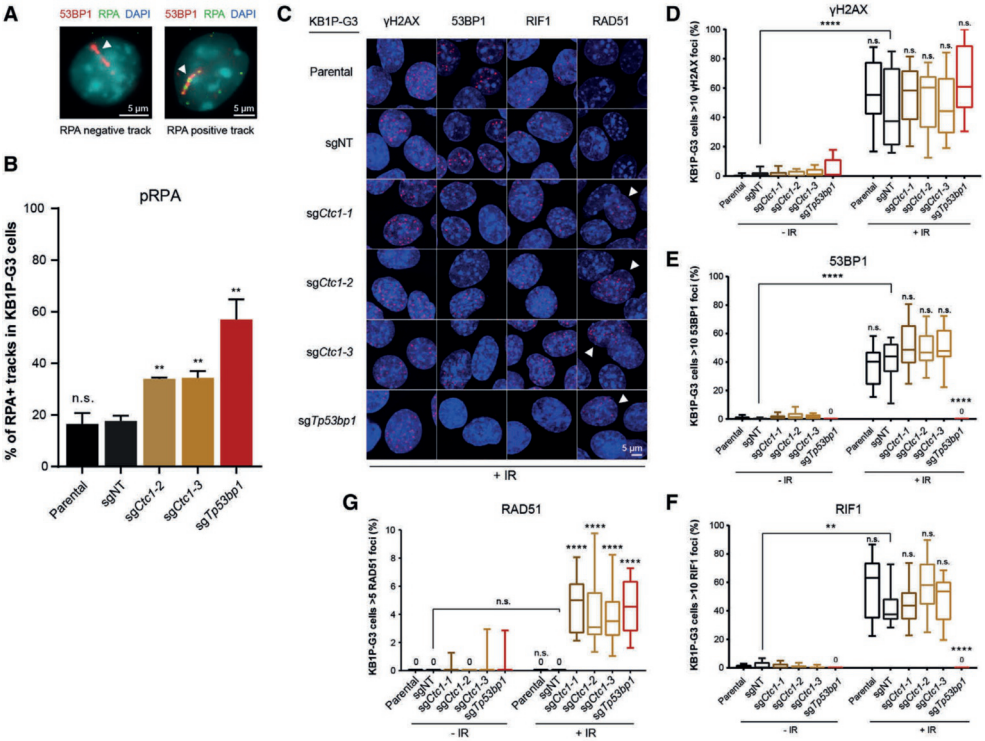

FIGURE 4 | CTC1 Functions as a Resection Antagonist on Non-telomeric DSBs. *(A-B)* CTC1 depletion induces RPA-coated ssDNA overhangs at sites of DNA damage in BRCA1-defient KB1P cells. *(A)* Representative images of RPA-negative and RPA-positive 53BP1-labeled alpha tracks in the indicated CRISPR/SpCas9-targeted KB1P-G3 cells (highlighted by the white arrowheads). Scale bars represent 5 µm. *(B)* RPA co-localization was quantified 1 hr after irradiation with an Americium-241 (^{241}Am) point source. The experiment was performed three times, and in each independent experiment, a minimum of 100 tracks were analyzed. Data are plotted as mean ± SEM. Significance was calculated by unpaired two-tailed Student's t test (**p < 0.01). *(C-G)* CTC1 depletion restores formation of DNA damage-induced RAD51 foci in BRCA1-deficient cells. *(C)* Representative confocal images of CRISPR/SpCas9-expressing KB1P-G3 cells targeted with the indicated sgRNAs. Cells were stained 3 hr after 10 Gy of ionizing radiation (IR) for the indicated proteins. RAD51-positive cells are highlighted by the white arrowheads. The scale bar represents 5 µm. *(D–G)* Quantification of confocal images, plotted as a box and whiskers plot. The box represents the 25th to 75th percentiles, and the whiskers show the minimum to maximum values. The experiment was performed at least twice, and data are plotted as a percentage of yH2AX- (D), 53BP1- (E), or RIF1-positive cells (> 10 foci) (F) or RAD51-positive cells (> 5 foci) (G) per field. Statistics were performed by Kruskal-Wallis non-parametric test followed by Dunn's multiple comparisons test. The indicated cell lines were compared with sgNT-treated cells (**** p < 0.0001). Also see Supplementary Fig. S3.

We next investigated whether CTC1 loss affects the recruitment of DDR factors to sites of irradiation-induced DNA damage. CRISPR/SpCas9-targeted KB1P-G3 cells were either left untreated or treated with 10 Gy of IR, which potently induced yH2AX foci (Fig. 4C-D; Supplementary Fig. S3A-B). Although depletion of 53BP1 in KB1P-G3 cells abolished the formation of IR-induced 53BP1 and RIF1 foci, these effects were not

observed in CTC1-depleted cells (Fig. 4E-F and S3C-D). Despite the capacity to form 53BP1 and RIF1 foci, KB1P-G3 cells that were depleted of CTC1 restored IR-induced RAD51 focus formation, whereas sgNT-transfected control cells were deficient for this activity (Fig. 4G-E). Similar conclusions were obtained when DNA damage was induced by treatment with 500 nM olaparib for 24 hr (Supplementary Fig. S3A,F–M). As expected, PARPi treatment resulted in more heterogeneous DNA damage induction compared with IR because PARP inhibition primarily exerts its cytotoxic effects during replication.

We then tested whether CTC1 loss resulted in productive HR events in conditional BRCA1-deficient $R26^{CreERT2}$;$Brca1^{SCo/\Delta}$;$Pim1^{DR\text{-}GFP/wt}$ mESC cells carrying a stably integrated DR-GFP reporter [41]. These cells were transfected to transiently express mCherry and I-SceI, and the percentage of mCherry/GFP double-positive cells was quantified by fluorescence-activated cell sorting (FACS) 24 hr later. Switching of the conditional $Brca1^{SCo}$ allele impaired HR activity, which was partially rescued upon depletion of the CST complex (Supplementary Fig. S3N-O).

Together, these data support a role for CTC1 as a resection antagonist acting on non-telomeric DSBs and as a mediator of the HR defect in BRCA1-deficient cells.

CTC1 Facilitates c-NHEJ-Mediated Repair at Telomeric and Non-Telomeric DSBs

It was previously shown that 53BP1, RIF1, and REV7/MAD2L2 antagonize resection and promote c-NHEJ [9, 10, 12-17]. However, this is not a universal phenotype for resection antagonists because it is not shared by HELB [40]. We therefore sought to determine whether CTC1 affects NHEJ activity. First, we used $Terf2^{-/-}$;$Trp53^{-/-}$ mouse embryonic fibroblasts (MEFs) that express a temperature-sensitive $TRF2^{Ile468Ala}$ mutant (TRF2ts) [31]. TRF2ts is functional and maintains intact TRF2-protected telomeres at 32°C, but it dissociates from telomeres at 37°C–39°C, inducing a DDR response and end-to-end chromosome fusions [31]. It was previously demonstrated that these fusions are driven by c-NHEJ and can be rescued by depletion of RNF8, LIG4, or REV7/MAD2L2 [16, 42-44].

We depleted CTC1 in TRF2ts MEFs grown under permissive conditions (Fig. 5A), which did not affect cell cycle distribution (Supplementary Fig. S4A-B). Cells were then grown at the non-permissive temperature (39°C) for 24 h to uncap telomeres and induce a DDR response prior to harvesting metaphase spreads for telomere fluorescence *in situ* hybridization (FISH). Although chromosome fusions were readily observed in control cells upon temperature-induced TRF2 inactivation, this was significantly reduced in *Ctc1*-mutated cells (Fig. 5B-C; Supplementary Fig. S4C–E). In line with this finding and with NHEJ being inhibited by long ssDNA overhangs, it was previously shown that depletion of CTC1 increased ssG overhang length [45, 46].

We next assessed whether CTC1 depletion in mouse CH12 B cells affects the ability to undergo class switch recombination (CSR) as a measure for non-telomeric c-NHEJ capacity [47]. CH12 cells were transfected with *Ctc1*-targeting CRISPR/SpCas9 constructs

and subcloned to obtain *Ctc1*-mutated CH12 cell clones. Notably, only 2 of 96 tested clones showed heterozygous *Ctc1* allele disruption, and no homozygous knockouts were obtained (Supplementary Fig. S4F-G), raising the possibility that complete loss of CTC1 is lethal in CH12 cells. Wild-type and heterozygous *Ctc1* knockout clones were subsequently stimulated with CD40Ab, interleukin-4 (IL-4), and transforming growth factor β-1 (TGF-β-1, CD40Ab, IL-4, and TGFβ-1 [CIT]) to induce CSR from immunoglobulin M (IgM) to IgA, which was monitored by flow cytometry. Interestingly, heterozygous knockout of *Ctc1* significantly diminished CSR in both

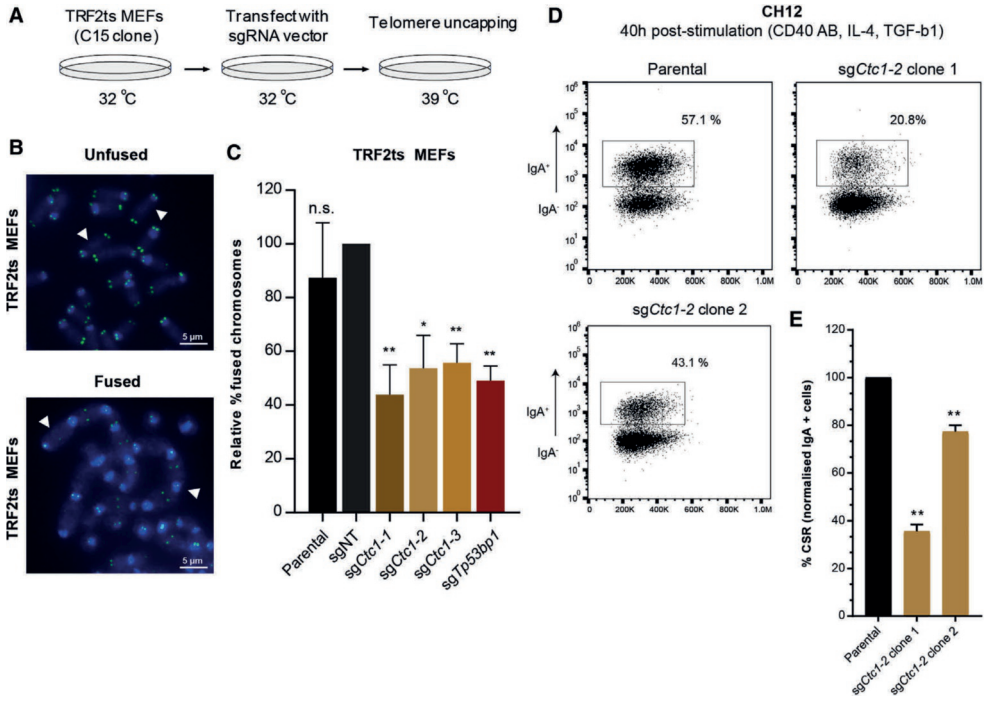

FIGURE 5 | CTC1 Facilitates c-NHEJ at Telomeric and Non-telomeric DSBs. *(A–C)* CTC1 depletion suppresses end-to-end fusions of uncapped telomeres. *(A)* Schematic overview of the telomere fusion assay. TRF2ts mouse embryonic fibroblasts (MEFs) of the indicated genotypes were cultured at the non-permissive temperature (39°C) for 24 hr before harvesting. *(B)* Representative images of metaphase spreads showing chromosomes unfused or fused at their telomeres (examples highlighted by white arrowheads). Chromosomes were stained with DAPI and a telomere-specific FISH probe (green). *(C)* Metaphases were detected and imaged automatically by Metafer. At least two independent experiments were performed, in each independent experiment, more than 2,000 chromosomes were counted manually. Genotypes were blinded during counting. Data are plotted as mean ± SEM. Significance was determined by unpaired two-tailed Student's t test ($^{*}p \leq 0.05$; $^{**}p \leq 0.01$). *(D-E)* Heterozygous inactivation of *Ctc1* impairs IgM-to-IgA class switch recombination (CSR) in CH12 B cells. *(D)* FACS analysis of CH12 clones of the indicated genotype 40 hr after induction of CSR by incubation with CD40Ab, IL-4, and TGF-β-1 (CIT). *(E)* Quantification of FACS data, representing mean ± SD of two independent experiments. Significance was calculated by unpaired Student's t test (** p value ≤ 0.01).

clones (Fig. 5D and 5E). We therefore conclude that CTC1 facilitates DSB repair via c-NHEJ at both telomeric and non-telomeric regions.

Depletion of CTC1 Mediates PARPi Resistance in the KB1P Mouse Model

Last, we explored the *in vivo* effects of CTC1 on the treatment response of BRCA1-deficient tumors to PARP inhibition. We analyzed whether *Ctc1* mRNA expression levels were altered in our previously generated collection of BRCA1- and p53-deficient KB1P and KB1PM mouse mammary tumors with acquired resistance to PARP inhibition [11]. In total, this collection comprises 60 treatment-naive tumors and 85 matched PARPi-resistant tumors derived from 23 unique donors. To examine the expression levels of *Ctc1* in treatment-naive and PARPi-resistant tumors, we produced RNA sequencing (RNA-seq) data for all tumors [48] and obtained the normalized expression values using edgeR [49]. We observed that the expression of *Ctc1* is significantly downregulated in PARPi-resistant tumors compared with naive tumors ($p = 6.34 \times 10^{-4}$) (Fig. 6A). Moreover, in tumors for which copy number variation by sequencing (CNVseq) data were available, CTC1 mRNA downregulation correlated with CNV loss (Supplementary Fig. S5A,D). Although a similar correlation was observed for STN1 and TEN1, these factors were not significantly downregulated in resistant tumors (Supplementary Fig. S5B-C,E-F).

Finally, we used mammary tumor organoid technology [50] to perform an *in vivo* intervention study with the PARPi olaparib in mice carrying tumors derived from isogenic KB1P organoids with or without disruption of *Ctc1*. For this purpose, KB1P4 organoids, derived from a KB1P mammary tumor, were cultured *ex vivo* and co-transduced with lentiviruses produced from pCMV-SpCas9 and pLenti-sg*Ctc1*-tetR-T2A-Puro vectors. Control organoids were generated by co-transduction with pCMV-SpCas9 and pLenti-sgNT-tetR-T2A-Puro lentivirus encoding a non-targeting sgRNA (Fig. 6B). The transduced KB1P4 tumor organoids were orthotopically transplanted in mice that were left untreated or treated daily with the PARPi olaparib for 56 consecutive days when tumors reached a size of 50–100 mm^3. As expected, the *Ctc1* target site was efficiently disrupted in tumors derived from KB1P4 organoids transduced with pCMV-SpCas9 and pLenti-sg*Ctc1*-tetR-T2A-Puro (Fig. 6C-D). Although KB1P4 control tumors only relapsed after treatment was stopped, CTC1-depleted tumors relapsed during treatment, resulting in accelerated mammary tumor-related death (median latencies: 39 days for sg*Ctc1_2* and 42 days for sg*Ctc1_3* cohorts compared with 73 days for control animals; log rank test, $p = 0.0019$ and $p = 0.0086$, respectively; Fig. 6E). These data confirmed that depletion of CTC1 confers PARPi resistance in BRCA1-deficient tumors *in vivo*.

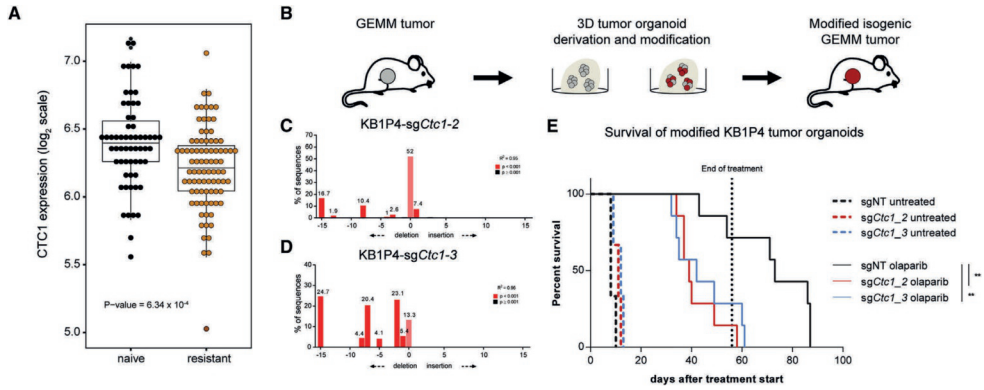

FIGURE 6 | Depletion of CTC1 Induces PARP Inhibitor Resistance *In Vivo*. *(A)* mRNA expression levels of Ctc1 in matched treatment-naive and PARPi-resistant BRCA1-deficient mouse mammary tumors. The y axis indicates the log2 (counts per million) value. *(B)* Schematic overview of the generation of isogenic Ctc1-mutated and control tumors via *ex vivo* manipulation of tumor organoids. *(C-D)* Example TIDE plots of untreated mammary tumors derived from Ctc1-mutated KB1P4 tumor organoids of the indicated genotype. *(E)* Survival of mice orthotopically transplanted with modified KB1P4 tumor organoids. Mice were stratified into untreated (n = 3) or olaparib-treated (100 mg/kg intraperitoneally daily for 56 consecutive days, n = 7) groups when tumors reached a size of 50–100 mm3. Significance was calculated by log rank (Mantel-Cox) test (**p < 0.01).

Discussion

In this study, we show that loss of the CST complex members CTC1, STN1, and TEN1 induces PARPi resistance in tumors with irreversible loss of function of BRCA1. Our data highlight the CST complex as a pathway for tumor cells to escape the synthetic lethal effects of PARPi by restoring HR independently of BRCA1. In particular, we demonstrate that the underlying mechanism is a restoration of end resection of DSBs. Together, our findings demonstrate that the CST complex contributes to the regulation of DNA end stability not only at telomeres but also at non-telomeric DSBs.

We and others have recently shown that the 53BP1-RIF1-REV7/MAD2L2 pathway is crucial for blocking end resection of DSBs [9, 10, 12-17]. However, it has remained elusive how DNA end stability is regulated by 53BP1-RIF1-REV7/MAD2L2 because none of these factors have been shown to contain direct DNA binding capacity and do not contain DNA processing activities. Our finding that the CST complex functions as a resection antagonist at DSBs sheds light on this puzzle. The CST complex is an RPA-like complex that can directly bind ssDNA via multiple OB folds [24]. In collaboration with the laboratory of Dan Durocher, we recently identified another RPA-like complex, the Shieldin (SHLD) complex, which is composed of SHLD1 (C20ORF196), SHLD2 (FAM35A), SHLD3 (FLJ26957/CTC-534A2.2), and REV7/MAD2L2, as a downstream effector of 53BP1 in DSB repair [51]. Hence, in addition to RPA and the SHLD complex, the CST complex is another trimeric complex that contains direct DNA binding capacity and affects DSB end stability. How these three complexes are recruited to DSBs in

time and space remains to be elucidated. Possibly, RPA, SHLD, and CST compete for ssDNA at resected DSBs or collapsed forks to either promote or antagonize HR. Not mutually exclusive with this model, it is conceivable that these complexes might contain specialized functions dependent on the ssDNA substrate since the CST complex has been reported to preferentially bind to and promote melting of G-rich regions and G4-quadruplexes [52, 53].

Future work is also required to elucidate whether these complexes form the final step in the regulation of DSB end stability (for instance, through steric hindrance) or whether additional downstream factors are involved. Intriguingly, the CST complex has been described to buffer resection at telomeres via POLA-dependent fill-in DNA synthesis, which is required to prevent excessive telomere erosion [22]. Our finding that the CST complex antagonizes resection at non-telomeric DSBs raises the question of whether this is dependent on POLA activity. Resection can possibly be antagonized not only by shielding the ends of DSBs from end-processing activities but also by directly counteracting ongoing resection via fill-in DNA synthesis. This buffering activity might fine-tune the length of ssDNA around the DSB, which is vulnerable for nucleolytic degradation, and it might provide a rescue mechanism in case HR cannot be completed.

The identification of the CST complex as a mediator of PARPi response in BRCA1-deficient tumors might also have clinical implications because loss-of-function mutations in the CST-encoding genes are predicted to cause clinical PARPi resistance. Moreover, we expect that these alterations provide therapeutic vulnerabilities because we recently found that depletion of the 53BP1-dependent DNA repair pathway enhances sensitivity to IR [54].

Materials and Methods

Cell Culture and Gene Editing

The KB1P-G3 cell line was previously established from a *K14cre;Brca1$^{F/F}$;Trp53$^{F/F}$* (KB1P) mouse mammary tumor and cultured as described by Jaspers et al. [11]. The KB2P-3.4 cell line was previously established from a *K14cre;Brca2$^{F/F}$;Trp53$^{F/F}$* (KB2P) mouse mammary tumor and cultured as described by Evers et al [55]. The KB1P4 3D tumor organoid line was previously established from a *Brca1$^{-/-}$;p53$^{-/-}$* mouse mammary tumor and cultured as described by Duarte et al [50] . Further *in vitro* culture details and gene editing details are provided in the Supplementary Materials and Methods.

Plasmids

Plasmids and cloning methods are provided in the Supplementary Materials and Methods.

PARPis

Olaparib (CAS 763113-22-0) and AZD2461 (CAS 1174043-16-3) were synthesized by and purchased from Syncom (Groningen, the Netherlands). Talazoparib was purchased from Selleckchem (catalog no.S7048).

Genomic DNA Isolation, PCR Amplification, and TIDE Analysis

Allele modification frequencies were quantified from genomic DNA isolated from tumor and cell line samples using Gentra Puregene (QIAGEN) according to the manufacturer's protocol. Target loci were amplified by PCR and submitted for Sanger sequencing to confirm target modification using the TIDE algorithm [36]. Parental cells were used as a reference sequence. PCR primer sequences are provided in Table S3. Further details are provided in the Supplementary Materials and Methods.

CRISPR Library Screens

Screening details are provided in the Supplementary Materials and Methods.

Alpha Track Assay

Experiments were performed as described previously [17] with minor modifications. Details are provided in the Supplementary Materials and Methods.

Focus Formation Experiments

RAD51 immunofluorescence in CRISPR/SpCas9-transfected KB1P-G3 cells was performed as described previously with minor modifications [17]. Details are provided in the Supplementary Materials and Methods.

DR-GFP

The DR-GFP was performed as described previously [41] Genes were targeted using the pLentiCRISPRv2 system containing the indicated sgRNAs.

Assessment of Telomere NHEJ

Trf2$^{-/-}$;*Trp53*$^{-/-}$;TRF2ts (TRF2ts) MEFs were described before [43], and metaphase chromosome analysis was done as described before [16]. Details are provided in the Supplementary Materials and Methods.

CSR Assay

Immunoglobulin CSR was performed as described previously [17]. Details are provided in the Supplementary Materials and Methods.

Generation of RNA-Seq Data

To determine the effects of Ctc1, Ten1, and Stn1 on PARPi treatment *in vivo*, we used RNA-seq dataset generated from a cohort of PARPi-naive and -resistant KB1P(M) tumors [11, 48]. Further details are provided in the Supplementary Materials and Methods.
Generation of CNV Sequencing Data

Genomic DNA was isolated from a subset of matched naive-and resistant KB1P-derived fresh-frozen tumor material using standard phenol:chloroform extraction [11, 48]. Further details are provided in the Supplementary Materials and Methods.

In Vivo Studies

All animal experiments were approved by the Animal Ethics Committee of the Netherlands Cancer Institute (Amsterdam, the Netherlands) and performed in accordance with the Dutch Act on Animal Experimentation (November 2014). Tumor organoids were allografted in 6- to 9-week-old female mice as described previously [50] with minor modifications. Further details are provided in the Supplementary Materials and Methods.

Quantification and Statistical Analysis

Statistical differences were calculated in GraphPad Prism using Student's t tests. Statistical significance in Fig. 2F was calculated by two-way ANOVA and *post hoc* Dunnett's correction for multiple comparisons and in Fig. 2G by one-way ANOVA and *post hoc* Dunnett's correction for multiple comparisons. Statistical differences in Fig. 4D–4G and Supplementary Fig. S3F–S3M were calculated by Kruskal-Wallis non-parametric test and *post hoc* Dunnett's correction for multiple comparisons. Statistical differences in Fig. 6E were calculated by log rank Mantel-Cox test. Significance is as follows: $p > 0.05$, not significant (n.s.); $^{*}p \leq 0.05$; $^{**}p \leq 0.01$; $^{***}p \leq 0.001$; $^{****}p \leq 0.0001$ unless otherwise stated in the figure legends. Original data files used to prepare the figures in this manuscript have been deposited in Mendeley Data and are available at https://doi.org/10.17632/6wyzgw8z8k.1.

Contact for Reagent and Resource Sharing

Further information and requests for resources and reagents should be directed to and will be fulfilled by S.R. (sven.rottenberg@vetsuisse.unibe.ch).

Data and Software Availability

The accession number for the raw data of RNA-seq and CNV sequencing reported in this paper is European Nucleotide Archive (ENA): PRJEB25803.

Acknowledgements

We wish to thank Piet Borst for critical reading of the manuscript, the members of the Preclinical Intervention Unit of the Mouse Clinic for Cancer and Aging (MCCA) at the Netherlands Cancer Institute (NKI) for their technical support with the animal experiments, and Julian R. de Ruiter for assistance with bioinformatic analysis. We are grateful to the NKI animal facility, digital microscopy facility, flow cytometry facility, and genomics core facility for their excellent service. Financial support came from the Dutch Cancer Society (KWF 2011-5220 and 2014-6532 to S.R. and J.J.), the Netherlands Organization for Scientific Research (VICI 91814643, NGI 93512009, Cancer Genomics Netherlands, and a National Roadmap Grant for Large-Scale Research Facilities to J.J. and STW 13577 to D.C.v.G.), the Swiss National Science Foundation (310030_156869 to S.R.), the Swiss Cancer League (KLS-4282-08-2017 to S.R.), the European Union (ERC StG 311565 to J.J.L.J., ERC CoG-681572 to S.R., and ERC Synergy Grant 319661 to J.J.), Cancer Research UK (CRUK/A14276 to C.J.L.), and a Breast Cancer Now Program Grant (CTR-Q4-Y2 to C.J.L.). R.C. and H.G. are supported by Cancer Research UK (C52690/A19270) and MRC (MR/M009971/1) grants, respectively, and a Wellcome core award (090532/Z/09/Z).

Author Contributions

Conceptualization, M.B., J.J., and S.R.; *Methodology*, M.B., S.A., S.J.P., B.E., and J.B.; *Software and Formal Analysis*, M.B., J.B., J.J., and S.R.; *Investigation*, M.B., S.A., S.J.P., I.d.K., H.G., S.J.R., C.L., J.F., F.F.S., and R.B.; *Resources,* B.E. and E.G.; *Writing*, M.B., J.J., and S.R.; *Supervision*, M.v.d.V., D.C.v.G., J.J.L.J., R.C., C.J.L., J.J., and S.R.; *Funding Acquisition*, D.C.v.G., J.J.L.J., R.C., C.J.L., J.J., and S.R.

Disclosure of Potential Conflicts of Interest

C.J.L. is a named inventor on patents describing the use of PARPis and stands to gain as part of the ICR's "Rewards to Investors" scheme.

References

1. Lord CJ, Ashworth A. PARP inhibitors: Synthetic lethality in the clinic. Science. 2017; 355: 1152-8.
2. Mateo J, Carreira S, Sandhu S, Miranda S, Mossop H, Perez-Lopez R, et al. DNA-Repair Defects and Olaparib in Metastatic Prostate Cancer. N Engl J Med. 2015; 373: 1697-708.
3. Pritchard CC, Mateo J, Walsh MF, De Sarkar N, Abida W, Beltran H, et al. Inherited DNA-Repair Gene Mutations in Men with Metastatic Prostate Cancer. N Engl J Med. 2016; 375: 443-53.
4. Patch AM, Christie EL, Etemadmoghadam D, Garsed DW, George J, Fereday S, et al. Whole-genome characterization of chemoresistant ovarian cancer. Nature. 2015; 521: 489-94.
5. Swisher EM, Sakai W, Karlan BY, Wurz K, Urban N, Taniguchi T. Secondary BRCA1 mutations in BRCA1-mutated ovarian carcinomas with platinum resistance. Cancer research. 2008; 68: 2581-6.
6. Ter Brugge P, Kristel P, van der Burg E, Boon U, de Maaker M, Lips E, et al. Mechanisms of Therapy Resistance in Patient-Derived Xenograft Models of BRCA1-Deficient Breast Cancer. J Natl Cancer Inst. 2016; 108.
7. Liu X, Holstege H, van der Gulden H, Treur-Mulder M, Zevenhoven J, Velds A, et al. Somatic loss of BRCA1 and p53 in mice induces mammary tumors with features of human BRCA1-mutated basal-like breast cancer. Proc Natl Acad Sci U S A. 2007; 104: 12111-6.
8. Rottenberg S, Jaspers JE, Kersbergen A, van der Burg E, Nygren AO, Zander SA, et al. High sensitivity of BRCA1-deficient mammary tumors to the PARP inhibitor AZD2281 alone and in combination with platinum drugs. Proc Natl Acad Sci U S A. 2008; 105: 17079-84.
9. Bouwman P, Aly A, Escandell JM, Pieterse M, Bartkova J, van der Gulden H, et al. 53BP1 loss rescues BRCA1 deficiency and is associated with triple-negative and BRCA-mutated breast cancers. Nat Struct Mol Biol. 2010; 17: 688-95.
10. Bunting SF, Callén E, Wong N, Chen HT, Polato F, Gunn A, et al. 53BP1 inhibits homologous recombination in Brca1-deficient cells by blocking resection of DNA breaks. Cell. 2010; 141: 243-54.
11. Jaspers JE, Kersbergen A, Boon U, Sol W, van Deemter L, Zander SA, et al. Loss of 53BP1 causes PARP inhibitor resistance in Brca1-mutated mouse mammary tumors. Cancer Discov. 2013; 3: 68-81.
12. Chapman JR, Barral P, Vannier JB, Borel V, Steger M, Tomas-Loba A, et al. RIF1 is essential for 53BP1-dependent nonhomologous end joining and suppression of DNA double-strand break resection. Mol Cell. 2013; 49: 858-71.
13. Di Virgilio M, Callen E, Yamane A, Zhang W, Jankovic M, Gitlin AD, et al. Rif1 prevents resection of DNA breaks and promotes immunoglobulin class switching. Science. 2013; 339: 711-5.
14. Escribano-Díaz C, Orthwein A, Fradet-Turcotte A, Xing M, Young JT, Tkáč J, et al. A cell cycle-dependent regulatory circuit composed of 53BP1-RIF1 and BRCA1-CtIP controls DNA repair pathway choice. Mol Cell. 2013; 49: 872-83.
15. Zimmermann M, Lottersberger F, Buonomo SB, Sfeir A, de Lange T. 53BP1 regulates DSB repair using Rif1 to control 5' end resection. Science. 2013; 339: 700-4.
16. Boersma V, Moatti N, Segura-Bayona S, Peuscher MH, van der Torre J, Wevers BA, et al. MAD2L2 controls DNA repair at telomeres and DNA breaks by inhibiting 5' end resection. Nature. 2015; 521: 537-40.
17. Xu G, Chapman JR, Brandsma I, Yuan J, Mistrik M, Bouwman P, et al. REV7 counteracts DNA double-strand break resection and affects PARP inhibition. Nature. 2015; 521: 541-4.
18. Panier S, Boulton SJ. Double-strand break repair: 53BP1 comes into focus. Nat Rev Mol Cell Biol. 2014; 15: 7-18.
19. Sfeir A, de Lange T. Removal of shelterin reveals the telomere end-protection problem. Science. 2012; 336: 593-7.
20. Makarov VL, Hirose Y, Langmore JP. Long G tails at both ends of human chromosomes suggest a C strand degradation mechanism for telomere shortening. Cell. 1997; 88: 657-66.
21. McElligott R, Wellinger RJ. The terminal DNA structure of mammalian chromosomes. Embo j. 1997; 16: 3705-14.
22. Lazzerini-Denchi E, Sfeir A. Stop pulling my strings - what telomeres taught us about the DNA damage response. Nat Rev Mol Cell Biol. 2016; 17: 364-78.
23. Feng X, Hsu SJ, Kasbek C, Chaiken M, Price CM. CTC1-mediated C-strand fill-in is an essential step in telomere length maintenance. Nucleic Acids Res. 2017; 45: 4281-93.

24. Miyake Y, Nakamura M, Nabetani A, Shimamura S, Tamura M, Yonehara S, et al. RPA-like mammalian Ctc1-Stn1-Ten1 complex binds to single-stranded DNA and protects telomeres independently of the Pot1 pathway. Mol Cell. 2009; 36: 193-206.
25. Wu P, Takai H, de Lange T. Telomeric 3' overhangs derive from resection by Exo1 and Apollo and fill-in by POT1b-associated CST. Cell. 2012; 150: 39-52.
26. Hom RA, Wuttke DS. Human CST Prefers G-Rich but Not Necessarily Telomeric Sequences. Biochemistry. 2017; 56: 4210-8.
27. Li W, Xu H, Xiao T, Cong L, Love MI, Zhang F, et al. MAGeCK enables robust identification of essential genes from genome-scale CRISPR/Cas9 knockout screens. Genome Biol. 2014; 15: 554.
28. Wang G, Zimmermann M, Mascall K, Lenoir WF, Moffat J, Angers S, et al. Identifying drug-gene interactions from CRISPR knockout screens with drugZ. bioRxiv. 2017: 232736.
29. Prahallad A, Heynen GJ, Germano G, Willems SM, Evers B, Vecchione L, et al. PTPN11 Is a Central Node in Intrinsic and Acquired Resistance to Targeted Cancer Drugs. Cell Rep. 2015; 12: 1978-85.
30. Oplustil O'Connor L, Rulten SL, Cranston AN, Odedra R, Brown H, Jaspers JE, et al. The PARP Inhibitor AZD2461 Provides Insights into the Role of PARP3 Inhibition for Both Synthetic Lethality and Tolerability with Chemotherapy in Preclinical Models. Cancer research. 2016; 76: 6084-94.
31. Koike-Yusa H, Li Y, Tan EP, Velasco-Herrera Mdel C, Yusa K. Genome-wide recessive genetic screening in mammalian cells with a lentiviral CRISPR-guide RNA library. Nat Biotechnol. 2014; 32: 267-73.
32. Elstrodt F, Hollestelle A, Nagel JH, Gorin M, Wasielewski M, van den Ouweland A, et al. BRCA1 mutation analysis of 41 human breast cancer cell lines reveals three new deleterious mutants. Cancer research. 2006; 66: 41-5.
33. Tzelepis K, Koike-Yusa H, De Braekeleer E, Li Y, Metzakopian E, Dovey OM, et al. A CRISPR Dropout Screen Identifies Genetic Vulnerabilities and Therapeutic Targets in Acute Myeloid Leukemia. Cell Rep. 2016; 17: 1193-205.
34. Pettitt SJ, Krastev DB, Brandsma I, Dréan A, Song F, Aleksandrov R, et al. Genome-wide and high-density CRISPR-Cas9 screens identify point mutations in PARP1 causing PARP inhibitor resistance. Nat Commun. 2018; 9: 1849.
35. Wang Y, Bernhardy AJ, Cruz C, Krais JJ, Nacson J, Nicolas E, et al. The BRCA1-Δ11q Alternative Splice Isoform Bypasses Germline Mutations and Promotes Therapeutic Resistance to PARP Inhibition and Cisplatin. Cancer research. 2016; 76: 2778-90.
36. Brinkman EK, Chen T, Amendola M, van Steensel B. Easy quantitative assessment of genome editing by sequence trace decomposition. Nucleic Acids Res. 2014; 42: e168.
37. Daley JM, Sung P. 53BP1, BRCA1, and the choice between recombination and end joining at DNA double-strand breaks. Mol Cell Biol. 2014; 34: 1380-8.
38. Bunting SF, Callén E, Kozak ML, Kim JM, Wong N, López-Contreras AJ, et al. BRCA1 functions independently of homologous recombination in DNA interstrand crosslink repair. Mol Cell. 2012; 46: 125-35.
39. Stap J, Krawczyk PM, Van Oven CH, Barendsen GW, Essers J, Kanaar R, et al. Induction of linear tracks of DNA double-strand breaks by alpha-particle irradiation of cells. Nat Methods. 2008; 5: 261-6.
40. Tkáč J, Xu G, Adhikary H, Young JTF, Gallo D, Escribano-Díaz C, et al. HELB Is a Feedback Inhibitor of DNA End Resection. Mol Cell. 2016; 61: 405-18.
41. Bouwman P, van der Gulden H, van der Heijden I, Drost R, Klijn CN, Prasetyanti P, et al. A high-throughput functional complementation assay for classification of BRCA1 missense variants. Cancer Discov. 2013; 3: 1142-55.
42. Celli GB, de Lange T. DNA processing is not required for ATM-mediated telomere damage response after TRF2 deletion. Nat Cell Biol. 2005; 7: 712-8.
43. Peuscher MH, Jacobs JJ. DNA-damage response and repair activities at uncapped telomeres depend on RNF8. Nat Cell Biol. 2011; 13: 1139-45.
44. Smogorzewska A, Karlseder J, Holtgreve-Grez H, Jauch A, de Lange T. DNA ligase IV-dependent NHEJ of deprotected mammalian telomeres in G1 and G2. Curr Biol. 2002; 12: 1635-44.
45. Chen LY, Redon S, Lingner J. The human CST complex is a terminator of telomerase activity. Nature. 2012; 488: 540-4.
46. Gu P, Min JN, Wang Y, Huang C, Peng T, Chai W, et al. CTC1 deletion results in defective telomere replication, leading to catastrophic telomere loss and stem cell exhaustion. Embo j. 2012; 31: 2309-21.

47. Muramatsu M, Kinoshita K, Fagarasan S, Yamada S, Shinkai Y, Honjo T. Class switch recombination and hypermutation require activation-induced cytidine deaminase (AID), a potential RNA editing enzyme. Cell. 2000; 102: 553-63.
48. Gogola E, Duarte AA, de Ruiter JR, Wiegant WW, Schmid JA, de Bruijn R, et al. Selective Loss of PARG Restores PARylation and Counteracts PARP Inhibitor-Mediated Synthetic Lethality. Cancer cell. 2018; 33: 1078-93.e12.
49. Robinson MD, McCarthy DJ, Smyth GK. edgeR: a Bioconductor package for differential expression analysis of digital gene expression data. Bioinformatics. 2010; 26: 139-40.
50. Duarte AA, Gogola E, Sachs N, Barazas M, Annunziato S, J RdR, et al. BRCA-deficient mouse mammary tumor organoids to study cancer-drug resistance. Nat Methods. 2018; 15: 134-40.
51. Noordermeer SM, Adam S, Setiaputra D, Barazas M, Pettitt SJ, Ling AK, et al. The shieldin complex mediates 53BP1-dependent DNA repair. Nature. 2018; 560: 117-21.
52. Bhattacharjee A, Wang Y, Diao J, Price CM. Dynamic DNA binding, junction recognition and G4 melting activity underlie the telomeric and genome-wide roles of human CST. Nucleic Acids Res. 2017; 45: 12311-24.
53. Lue NF, Zhou R, Chico L, Mao N, Steinberg-Neifach O, Ha T. The telomere capping complex CST has an unusual stoichiometry, makes multipartite interaction with G-Tails, and unfolds higher-order G-tail structures. PLoS Genet. 2013; 9: e1003145.
54. Barazas M, Gasparini A, Huang Y, Küçükosmanoğlu A, Annunziato S, Bouwman P, et al. Radiosensitivity Is an Acquired Vulnerability of PARPi-Resistant BRCA1-Deficient Tumors. Cancer research. 2019; 79: 452-60.
55. Evers B, Drost R, Schut E, de Bruin M, van der Burg E, Derksen PW, et al. Selective inhibition of BRCA2-deficient mammary tumor cell growth by AZD2281 and cisplatin. Clinical cancer research : an official journal of the American Association for Cancer Research. 2008; 14: 3916-25.

Supplementary Materials and Methods

Cell culture

KB1P and KB2P mouse mammary tumor cell lines were cultured in DMEM/F-12 medium (Life Technologies) in the presence of 10% FCS, penicillin/streptomycin (Gibco), 5µg/mL insulin (Sigma), 5ng/mL epidermal growth factor (Life Technologies) and 5ng/mL cholera toxin (Gentaur) under low oxygen conditions (3% O_2, 5% CO_2 at 37°C). SUM149PT cells were cultured in Ham's F12 medium (Gibco) supplemented with 5% FCS, 5 µg/ml insulin, 1 µg/mL hydrocortisone (Sigma-Aldrich, St. Louis, MI, USA). Mouse ES cells with a selectable conditional *Brca1* deletion (*R26*$^{CreERT2/wt}$*;Brca1*$^{SCo/\Delta}$ and *R26*^{CreERT2}*;Brca1*$^{SCo/\Delta}$*; Pim1*$^{DR\text{-}GFP/wt}$) [1, 2] were cultured on gelatin-coated plates in 60% buffalo red liver (BRL) cell conditioned medium supplied with 10% fetal calf serum, 0.1 mM β-mercaptoethanol (Merck) and 10^3 U/ml ESGRO LIF (Millipore) under normal oxygen conditions (21% O_2, 5% CO_2, 37°C). *Trf2*$^{-/-}$*p53*$^{-/-}$ TRF2ts MEFs were grown in DMEM with 100U penicillin, 0.1 mg/ml streptomycin, 2mML-glutamine and 10%FBS. TRF2ts MEFs were maintained at the permissive temperature of 32 °C and only grown at 39°C to induce telomere uncapping through inactivation of TRF2 [3]. CH12F3 cell lines were cultured in RPMI supplemented with 5 % NCTC-109 medium, 10% FCS, 100 U/ml penicillin, 100 ng/ml streptomycin and 2 mM L-glutamine at 37°C with 5% CO_2 under ambient oxygen conditions. KB1P4 3D tumor organoid cells were seeded in Basement Membrane Extract Type 2 (BME, Trevigen) on 24-well suspension plates (Greiner Bio-One) and cultured in AdDMEM/F12 supplemented with 1 M HEPES (Sigma), GlutaMAX (Invitrogen), penicillin/

streptomycin (Gibco), B27 (Gibco), 125 µM N-acetyl-L- cysteine (Sigma), 50 ng/mL murine epidermal growth factor (Invitrogen).

Transfection-based genome editing

Transfection in KB1P-G3 cells was performed using TransIT-LT1 (Mirus) reagents following manufacturer's recommendations. In brief, 150,000 cells were plated in 6-well format 1 day before transfection with 1 µg DNA. The medium was refreshed 24 hours after transfection and transfected cells were selected with puromycin for three days. CRISPR/SpCas9 targeted SUM149PT cells were generated with editR crRNA (Dharmacon, Lafayette, CO, USA).

Lentiviral transduction-based genome editing

Cell lines targeted with the pGSC_Cas9_Neo and pLenti-sgRNA-tetR-T2A-Puro system were generated by lentiviral transduction. Lentivirus was produced in HEK293FT cells as described previously [4] and mouse KB1P-G3 or *Brca1*$^{-/-}$;*p53*$^{-/-}$ mES cells were infected overnight using polybrene (8 µg/mL). The medium was refreshed after 12 hours and transduced cells were selected with puromycin (3 µg/mL) and blasticidin (500 µg/mL) for five consecutive days. KB1P4 tumor organoids were transduced using spinoculation as described previously [5, 6]. Expression of the sgRNA was induced by incubation with 3 µg/ml doxycycline (Sigma) for at least five days.

Plasmids

pGSC_Cas9_Neo and pLenti-sgRNA-tetR-T2A-Puro were described previously [7]. Genome- wide mouse lentiviral CRISPR sgRNA library was a gift from Kosuke Yusa (Addgene #50947). Human Improved Genome-wide Knockout CRISPR Library v1 was a gift from Kosuke Yusa (Addgene #67989). pX330-U6- Chimeric_BB-CBh-SpCas9 was a gift from Feng Zhang (Addgene plasmid #42230). pLentiCRISPRv2 was a gift from Feng Zhang (Addgene plasmid # 52961). The MCherry/I-SceI plasmid has been described previously [2].

Generation of CRISPR/SpCas9 plasmids

Unless otherwise stated, KB1P-G3 experiments were performed using a modified version of the pX330 backbone [8] in which a puromycin resistance ORF was cloned under the hPGK promoter [9]. sgRNA sequences were cloned in the pX330puro backbone using custom DNA oligos (IDT) which were melted, annealed and subsequently ligated with quick-ligase (NEB) into BbsI-digested backbone. A similar procedure was used for cloning into the pLenti-sgRNA-tetR-T2A-Puro vector, but using

BfuAI-digested backbone. All constructs were sequence verified by Sanger sequencing. sgRNA sequences are provided in Supplementary Table S2.

Genomic DNA isolation, PCR amplification and TIDE analysis

Target loci were amplified by PCR using the following conditions: (1) 98 °C, 30 s, (2) 30 cycles of 98 °C for 10 s, 61 °C for 20 s and 72 °C for 30 s, (3) 72 °C, 5 min. Reaction mix consisted of 0.75 µl DMSO, 5 µl GC Phusion Buffer 5X, 0.5 µl 2 mM dNTPs, 0.125 µl 100 µM Fwd oligo, 0.125 µl 100 µM Rev oligo, 0.25 µl Phusion polymerase in 25 µl total volume. Amplified products were diluted 50X in dH_2O and 2 µl of diluted product was submitted for Sanger sequencing.

CRISPR library screens

The first PARPi resistance screen was performed in the KB1P-G3 tumor cell line, which was previously established from a KB1P tumor [10]. This cell line is BRCA1- and p53-deficient through large intragenic deletions and shows sensitivity to PARPi treatment in the nanomolar range. The DDR sgRNA library was generated based on the gene list from Thanos Halazonetis (University of Geneva) described before [11, 12] and the NCBI search (terms: "DNA repair", "DNA damage response", "DNA replication", "telomere- associated genes"). See Table S1 for the full library details. This search resulted in a DDR-related gene list comprising a total of 1,752 genes (Supplementary Table S1). *Tp53bp1* was specifically removed from this list in anticipation that loss of 53BP1 might dominate the screen results and thereby obscure the effects of other genes. sgRNAs targeting the 1,752 DDR-related genes were synthesized (MYcroarray) and cloned into the pLenti-sgRNA-tetR-T2A-PuroR vector, which allows for doxycycline inducible expression of the sgRNA [7]. KB1P-G3-SpCas9 expressing cells were generated by transduction with the pGSC_SpCas9_Neo vector and transduced cells were selected by 500 µg/mL G418. The pLenti-sgRNA-tetR-T2A-Puro-DDR library was introduced at 100x coverage. Next, doxycycline was added to the medium for 5 days to mutagenize the population. Cells were subsequently plated in a clonogenic growth format in the presence of the PARP inhibitors olaparib or AZD2461 [13] at the approximate IC90 concentration for 14 days. Cells were harvested before and after PARPi treatment for genomic DNA isolation. Subsequently, sgRNA sequences were amplified from genomic DNA by two rounds of PCR amplification as described [5] and sequenced with the HiSeq 2500, using the following barcodes: GTAGCC, TACAAG, CTCTAC, GCGGAC, TTTCAC, GGCCAC. Sequencing reads were aligned to the reference sequences using edgeR software [14]. The screening data were processed by the MAGeCK algorithm [15], and results were sorted on MAGeCK-based positive selected gene ranks to allow comparison across screens.

The second PARPi resistance screen was performed in BRCA1- and p53-deficient, SpCas9-expressing mouse embryonic stem (mES) cells infected with a genome-wide lentiviral sgRNA library targeting 19,150 genes [16]. The screen was performed at 75x coverage in two independent transductions (MOI 0.5) and cells were first selected with puromycin and subsequently treated with olaparib at a concentration of 15 nM for 10 days. Surviving populations were harvested and processed as described previously [16], using the following barcodes CGTGAT, ACATCG, GCCTAA, TGGTCA, CACTGT, ATTGGC, GATCTG, TCAAGT, CTGATC, AAGCTA, GTAGCC, TACAAG, TTGACT, GGAACT. The screening data were processed similar to the screen in KB1P-G3 cells.

A third PARPi resistance screen was performed in the SUM149PT human breast cancer cell line. This cell line harbors the *BRCA1*^{2288delT} mutation and LOH [17]. A derivative of SUM149PT with an integrated tetracycline-inducible SpCas9 was lentivirally infected with a genome-wide sgRNA library designed to target 18,010 genes [18] using a multiplicity of infection of 0.3 and infecting >1000 cells per sgRNA. After puromycin selection (3 µg/ml) to remove non-tranduced cells, a sample was removed (time or t=0); remaining cells were cultured in the presence or absence of doxycycline plus 100 nM talazoparib, a concentration which normally results in complete inhibition of the cell population. No cells survived in the absence of doxycycline. After two weeks of selection, genomic DNA from the remaining cells in the doxycycline-treated sample was recovered. The sgRNA sequences from this genomic DNA were PCR amplified using barcoded and tailed primers and deep sequenced as previously described [16] to identify sgRNAs in the talazoparib-resistant population. Read counts were normalized for coverage by converting to parts per ten million (pptm) reads and fold change between starting and resistant population was calculated for each guide. Fold change values were log- and Z- transformed and plotted based on z-rank [19].

Clonogenic survival assay

Ctc1, *Stn1* and *Ten1* were targeted in *R26*^{CreERT2}*;Brca1*$^{SCo/\Delta}$ mouse embryonic stem (mES) cells using pLentiCRISPRv2 vectors, Cre-mediated inactivation of the endogenous mouse *Brca1*^{SCo} allele was achieved by overnight incubation of cells with 0.5 µmol/L 4-OHT (Sigma) [1]. Four days after switching, cells were seeded in triplicate at 10,000 cells per well in 6-well plates for clonogenic survival assay. For experiments with *R26*$^{CreERT2/wt}$*; Brca1*$^{SCo/\Delta}$ p53-null cells, cells were plated without treatment or in the presence of olaparib 2.5 nM. Cells were stained with 0.1% crystal violet one week later, and scanned with the Gelcount (Oxford Optronix). Automated quantification of colony counts was performed using the Gelcount colony counter software.

Clonogenic survival assay with PARPi (olaparib) were performed as described previously with minor modifications [12]. CRISPR/SpCas9 transfected KB1P-G3 cells were seeded in triplicate at 5 x 10^3 cells per well into 6-well plates on day 0, and

then olaparib or AZD2461 was added at the indicated concentrations. On day 6, the untreated group was fixed, the other groups were fixed on day 9 and stained with 0.1% crystal violet. Plates were scanned with the Gelcount (Oxford Optronix). Quantifications were performed by solubilizing crystal violet using 10% acetic acid and the absorbance at 562nm was measured using the Tecan plate reader. The experiment was performed three times.

SUM149PT-SpCas9 cells were transfected with *CTC1* targeting crRNA and tracrRNA using the EditR system (Life Technologies), plated into 48 well plates and then treated with 50 nM talazoparib. Medium was replaced with fresh drug-containing medium as indicated. Images were taken to measure viability of cells in each well every 12 hours using the IncuCyte system. After two weeks, final viability was assessed using CellTiter Glo (Promega).

Competition assays

Competition assays were performed in KB1P-G3 SpCas9 expressing cells, transduced with pLenti-sgRNA-tetR- T2A-Puro vectors containing the indicated sgRNAs. Cells were selected with puromycin (3 µg/mL) for three days and allowed to recover from selection. A sample was harvested for gDNA isolation at t = 0, and 5,000 cells were plated in 6-well plates in triplicate per condition, with or without AZD2461 (250 nM). After 10 days of treatment, cells were harvested, counted and re-plated at 5,000 cells per 6-well two times (total treatment time of 30 days). On the last time point, each condition was plated as technical duplicate. At the end point, one technical duplicate well was fixed and stained with crystal violet and the other was used to isolate gDNA. Allele distributions were determined from gDNA samples by PCR followed by Sanger sequencing and TIDE analysis, as described above. Competition assays in KB2P-3.4 cells were performed similarly, except 2,000 cells were seeded per 6-well and cells were treated with olaparib (50 nM).

Growth curves

Growth curves were generated for CRISPR/SpCas9 transfected KB1P-G3 cells by seeding 1,000 cells per well in 96-well plates, seeding 6 technical replicates per experiment and the well confluency was recorded every 4 hours for 120 hours using an IncuCyte Zoom Live – Cell Analysis System (Essen Bioscience). The images were analyzed using IncuCyte Zoom software. Data were normalized to the confluency at 20h after seeding.

Alpha track assay

Experiments were performed as described previously [12] with small modifications. CRISPR/SpCas9 transfected KB1P-G3 cells were seeded on coverslips overnight, washed

with PBS and covered with a mylar foil, allowing α-particle irradiation from above, through mylar. Irradiation was done using a ^{241}Am point- source by moving the source over the coverslip for 30s per area, cells were incubated for 1 hour at 37 ˚C and washed with ice- cold PBS. Subsequently, cells were extracted with cold CSK buffer (10 mM HEPES-KOH, pH 7.9, 100 mM NaCl, 300 mM sucrose, 3 mM MgCl2, 1 mM EGTA, 0.5% (v/v) Triton X-100) and cold CSS buffer (10 mM Tris, pH 7.4, 10 mM NaCl, 3 mM MgCl2, 1% (v/v) Tween20, 0.5% (w/v) sodium deoxycholate) for 5 min each before fixation in 4% PFA in PBS for 30 min at room temperature. Fixed cells were washed 2 times for 10 minutes in PBS (0.1% Triton X-100) and washed for 30 minutes in blocking solution (0.5% BSA and 0.15% glycine in PBS). Primary antibodies were diluted in blocking buffer and incubated overnight at 4 ˚C. Hereafter, cells were washed 2 times for 10 minutes in PBS (0.1% Triton X-100) and 1 time shortly in blocking buffer. Secondary antibodies were diluted in blocking buffer and cells were incubated for at least 1 hour at room temperature in the dark. Finally, cells were washed 2 times in PBS and coverslips were mounted using Vectashield with DAPI. Quantification was done as described previously. Primary antibodies used in this study were as follows: rabbit anti-53BP1 (NB100-304, Novus), 1:1000 dilution; mouse anti-RPA34-20 (Ab-3, CalBiochem), 1:1000 dilution; MRE11 antibody [20], 1:250 dilution. Secondary antibodies used in this study were as follows: Alexa Fluor 594 goat anti-rabbit IgG (A 31631, Invitrogen), Alexa Fluor 488 goat anti-mouse IgG (Thermo Fisher Scientific Cat# A-11001, RRID: AB_2534069), 1:1000 dilution.

Foci formation experiments

RAD51 immunofluorescence in CRISPR/SpCas9 transfected KB1P-G3 cells was performed as described previously, with minor modifications [12]. Cells were grown on 8-well chamber slides (Millipore). Ionizing-Radiation Induced Foci (IRIF) were induced by γ-irradiation (10 Gy) 3 hours prior to sample preparation. PARP inhibitor-induced foci were generated by treatment with 500 nM olaparib for 24h prior to sample preparation. Subsequently, cells were washed in PBS++ and fixed with 2% PFA/PBS++ for 20' on ice. Fixed cells were washed with PBS++ and were permeabilized for 20' in 0.2% Triton X-100/PBS++. All subsequent steps were performed in staining buffer (PBS++, BSA (2%), glycine (0.15%), Triton X-100 (0.1%)). Cells were washed 3x and blocked for 30' at RT, incubated with the 1st antibody for 2hrs at RT, washed 3x and incubated with the 2nd antibody for 1hr at RT. Antibodies were diluted in staining buffer. Last, cells were mounted and counterstained using Vectashield mounting medium with DAPI (H1500, Vector Laboratories). Primary antibodies used: rabbit-anti-RAD51; 70-001, BioAcademia, 1:1,000 dilution; rabbit-anti-53BP1; Abcam Ab21083, 1:2,000 dilution; rabbit-anti-RIF1 was a gift by Ross Chapman, 1:1,000 dilution; mouse anti yH2AX: Millipore JBW3O1, 1:1,000 dilution; Alexa fluor 568 F(ab')$_2$ Fragment goat anti-rabbit; A21069, Thermo Fisher Scientific,

1:400 dilution; Goat anti-Rabbit IgG (H+L) Cross-Adsorbed Secondary Antibody, Alexa Fluor 568 from Thermo Fisher Scientific, catalog # A-11011, RRID AB_143157; Goat anti-Mouse IgG (H+L) Cross-Adsorbed Secondary Antibody, Alexa Fluor 568 from Thermo Fisher Scientific, catalog # A-11004, RRID AB_2534072. Z-stack images were acquired using a confocal microscope (Leica SP5, Leica Microsystems GmbH) and multiple different confocal fields were imaged per sample (63x objective). Confocal images were analyzed automatically using an ImageJ script [12]. Briefly, the macro detects nuclei based on DAPI intensity and subsequently counts the number of foci within each nucleus.

DR-GFP

The DR-GFP assay was performed as described previously [2]. Genes were targeted using the pLentiCRISPRv2 system containing indicated sgRNAs.

Assessment of telomere NHEJ

Trf2$^{-/-}$*;Trp53*$^{-/-}$;TRF2ts MEFs (TRF2ts MEFs) were described before [3]. TRF2ts MEFs were targeted using the pX330puro system containing indicated sgRNAs at the permissive temperature of 32°C. Following selection and recovery, they were grown for 24 h at the non-permissive temperature of 39°C to inactivate TRF2 and induce NHEJ dependent chromosome end to end fusions as a consequence of telomere uncapping. Cell harvesting, preparation of metaphase spreads and telomere FISH with an Alexa488-labeled C-rich Telomere probe (PN-TC060-005, Panagene/Eurogentec) for metaphase chromosome analysis was done as described before [21].

Digital images of metaphases were captured using the Metafer4/MSearch automated metaphase finder system (MetaSystems, Germany) equipped with an AxioImager Z2 microscope (Carl Zeiss, Germany). After scanning metaphase preparations at 10x magnification, high-resolution images of metaphases were acquired using a 'Plan-Apochromat' 63x/1,40 oil objective. The cell cycle distribution of TRF2ts MEFs with or without CRISPR/SpCas9 mediated disruption of *Ctc1* or *Tp53bp1* was determined by propidium-iodide staining, acquired on a FACSCalibur (Beckton Dickinson) and analyzed with FlowJo (TreeStar, Ashland, OR) software.

CSR assay

Ctc1-mutated CH12F3 cells were generated by nucleofection (Amaxa Nucleofector 2b, Lonza) with 2 µg of plasmid and Cell Line Nucleofector Kit R (Lonza), using program D-023. Isogenic cell clones were isolated by limiting dilution and mutated clones were identified by native PAGE resolution of PCR amplicons of the target site, and subsequent confirmation by Sanger sequencing. Immunoglobulin CSR

was performed as described previously [12]. Briefly, CH12 cells were either mock-treated or stimulated with agonist anti-CD40 antibody (0.5 mg/ml; eBioscience; HM40-3), mouse IL-4 (5 ng/ml; R&D Systems) and TGF-b1 (1.25 ng/ml; R&D Systems). Cell- surface IgA expression was determined by flow cytometry, immunostaining with biotinylated antimouse IgA antibody (eBioscience; 13-5994), and Alexa488-streptavidin conjugate (Life Technologies).

Generation of RNA sequencing data

To determine the effects of Ctc1, Ten1 and Stn1 on PARPi treatment *in vivo*, we used our RNASeq dataset generated from a cohort of PARPi-naive and -resistant KB1P and KB1PM tumors [10, 22]. Hereto, fresh-frozen tumor tissues were subjected to high-speed shaking in 2 ml microcentrifuge tubes containing 1 ml of TRIsure reagent (Bioline) and stainless-steel beads (TissueLyser LT, Qiagen; 10 min, 50 Hz, room temperature). Homogenized lysates were further processed for RNA isolation following TRIsure manufacturer's protocol. Quality and quantity of the total RNA was assessed by the 2100 Bioanalyzer using a Nano chip (Agilent, Santa Clara, CA). Total RNA samples having RIN>8 were subjected to library generation. Strand- specific libraries were generated using the TruSeq Stranded mRNA sample preparation kit (Illumina Inc., San Diego, RS-122-2101/2) according to the manufacturer's instructions (Illumina, Part # 15031047 Rev. E). The libraries were analyzed on a 2100 Bioanalyzer using a 7500 chip (Agilent, Santa Clara, CA), diluted and pooled equimolar into a 10 nM sequencing stock solution. Ilumina TruSeq mRNA libraries were sequenced with 50 base single reads on a HiSeq2000 using V3 chemistry (Illumina Inc., San Diego). The resulting reads were trimmed using Cutadapt v.1.12. The trimmed reads were aligned to the GRCm38 reference genome using STAR v.2.5.2b [23]. QC statistics from Fastqc v.0.11.5 (www.bioinformatics.babraham.ac.uk/projects/fastqc) and the above-mentioned tools were collected and summarized using Multiqc (v.0.8; [24]). Gene expression counts were generated by featureCounts (v.1.5.2; [25]) using gene definitions from Ensembl GRCm38 version 76. The genes with counts per million (CPM) larger than one at least 20% of total number of samples were taken and used for further analysis. Then, trimmed mean of M-value (TMM) normalization was performed to obtain normalized expression using edgeR [14].

Generation of CNV sequencing data

CNV-Seq was performed using double stranded DNA (dsDNA), quantified with the Qubit® dsDNA HS Assay Kit (Invitrogen, #Q32851). To obtain fragment sizes of 160–180 bp, 2 µg of dsDNA were fragmented by Covaris shearing and purified using 1.8X Agencourt AMPure XP PCR Purification beads according to manufacturer's protocol (Beckman Coulter, #A63881). Next, sheared DNA was quantified and qualified

on a BioAnalyzer system with the DNA7500 assay kit (Agilent Technologies, #5067-1506). Library preparation for Illumina sequencing was carried out with 1 µg of DNA and KAPA HTP Library Preparation Kit (KAPA Biosystems, #KK8234). HiSeq2500 machine in one lane of a single read 65 bp run, according to manufacturer's instructions. Sequencing reads were trimmed using Cutadapt (version 1.12) and reads shorter than 30 bp were removed. The trimmed reads were aligned to the GRCm38 reference genome using BWA (version 0.7.15; [26]). The resulting alignments were sorted and marked for duplicates using Picard tools (version 2.5.0). Copy number calls were generated using the QDNAseq and QDNAseq.mm10 [27] packages from Bioconductor (versions 1.8.0 and 1.4.0, respectively). Copy number calls of the resistant tumors were subtracted to those of matched naïve tumors for downstream analysis which examined the correlation between CNV and gene expression.

In vivo studies

Tumor organoids were collected, incubated with TripLE at 37°C for 5', dissociated into single cells, washed in PBS, resuspended in tumor organoid medium and mixed in a 1:1 ratio of tumor organoid suspension and BME in a cell concentration of 10^4 cells per 40 µl. Subsequently, 10^4 cells were transplanted in the fourth right mammary fat pad of 6–9-week-old NMRI nude mice. Mammary tumor size was measured by caliper measurements and tumor volume was calculated (0.5 x length x width^2). Treatment of tumor bearing mice was initiated when tumors reached a size of 50-100 mm^3, at which point mice were stratified into the untreated (n = 3) or olaparib treatment group (n = 7). Olaparib was administered at 100 mg/kg intraperitoneally for 56 consecutive days. Animals were sacrificed with CO_2 when the tumor reached a volume of 1,500 mm^3.

Supplementary Figures and Tables

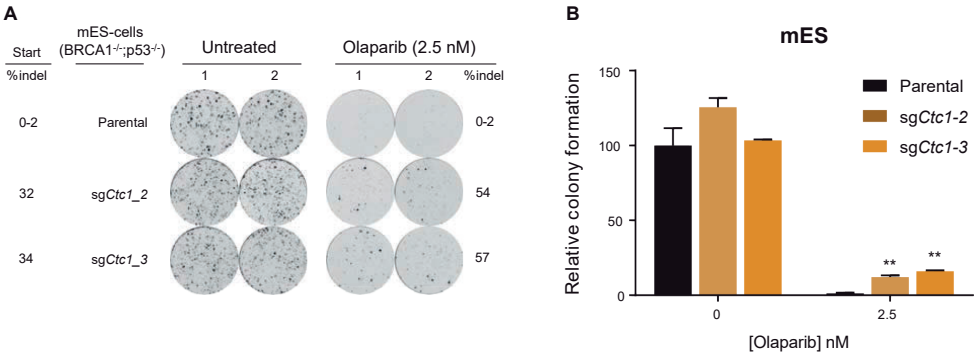

SUPPLEMENTARY FIGURE S1 | Depletion of CTC1 induces PARPi resistance in *Brca1*$^{-/-}$;*p53*$^{-/-}$ mouse embryonic stem (mES) cells. Related to Figure 3. *(A)* Parental and *Ctc1*-mutated *Brca1*$^{-/-}$;*p53*$^{-/-}$ mES cells were plated for clonogenic growth in the presence or absence of olaparib (2.5 nM) for 7 days before wells were fixed and stained with crystal violet. The experiment was performed in duplicate. *Ctc1* was mutated using the pLenti-sgRNA-tetR-T2A-PuroR vector containing the indicated gRNAs. Allele distributions were determined from the starting population and the surviving population after treatment. *(B)* Quantification of A. The number of colonies was determined using GelCount software. Data represent the relative number of colonies compared to the parental untreated mES cells. Data represent mean ± SD. P-values were determined by unpaired two-tailed students t-test (P = 0.0074 and P = 0.0017, respectively).

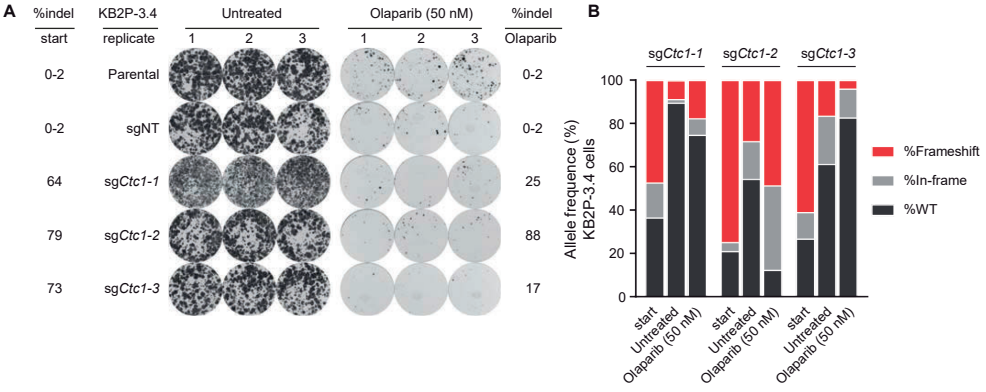

SUPPLEMENTARY FIGURE S2 | Depletion of CTC1 does not improve PARPi survival in BRCA2-deficient cells. Related to Figure 3. *(A-B)* Parental, sgNT or *Ctc1*-mutated KB2P-3.4 SpCas9 expressing cells were plated at 2,000 cells per 6-well for clonogenic growth in the presence or absence of olaparib (50 nM) for 10 days. Then, cells were harvested and re-plated at 2,000 cells per 6-well under the same treatment for 10 days, and this was repeated one more time (total treatment duration 30 days). *Ctc1* was mutated using the pLenti-sgRNA-tetR-T2A-PuroR vector containing the indicated gRNAs. Cells were selected with puromycin (3 µg/mL) and gRNA expression was induced with doxycycline (3 µg/mL) for 5 days. Allele distributions were determined from the starting, untreated and olaparib-treated populations and the percentage indel is shown and plotted in *B*.

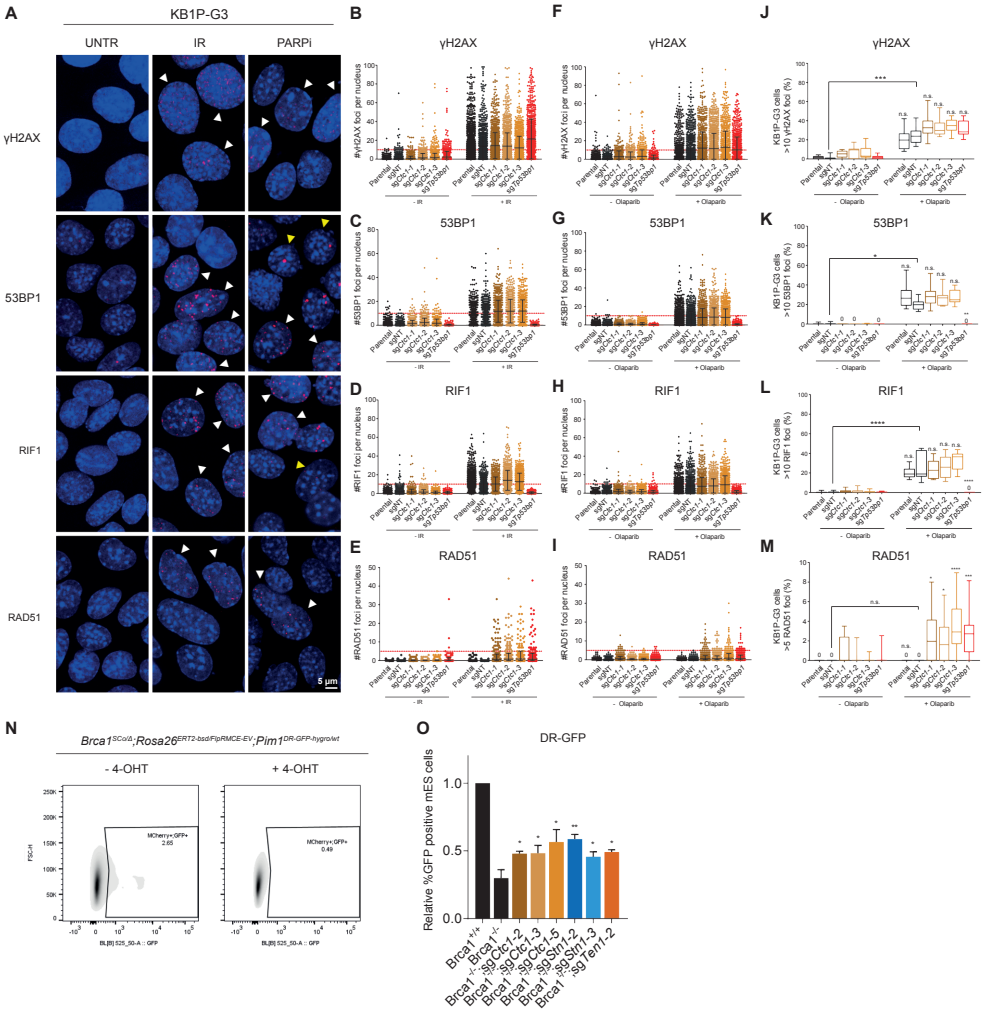

SUPPLEMENTARY FIGURE S3 | CTC1 functions as a resection antagonist on non-telomeric DSBs. Related to Figure 4. *(A)* Overview confocal images (63x magnification) of indicated proteins and treatments. White arrowheads indicate examples of positive cells, and yellow arrowheads indicate examples of negative cells containing nuclear bodies. *(B-E)* Quantifications of confocal images shown in Figure 4C. KB1P-G3 SpCas9 expressing cells of indicated genotype were irradiated (10 Gy) and harvested 3 hours later for immunofluorescence of indicated proteins. Data is plotted as #foci per nucleus for indicated proteins. *(F-M)* Immunofluorescence stainings were performed after 500nM olaparib treatment for 24h to induce DSBs. Data represent two independent experiments. *F-I* show quantifications of confocal images plotted as #foci per nucleus for indicated proteins, *J-M* quantification of confocal images, plotted as box and whiskers plot. The box represents the 25th to 75th percentiles and the whiskers show the min to max values. The experiment was performed at least two times and data is plotted as percentage of γH2AX, 53BP1 or RIF1-positive cells (>10 foci) or RAD51-positive cells (>5 foci) per field. Statistics was performed by Kruskal-Wallis non-parametric test followed by Dunn's multiple comparisons test. The indicated cell lines were compared to sgNT treated cells (**** = p-value < 0.0001). *Figure legend continues on next page.*

SUPPLEMENTARY FIGURE S3 | CTC1 functions as a resection antagonist on non-telomeric DSBs. Related to Figure 4. *Continued. (N-O)* CST complex members were depleted in *Brca1*$^{SCo/\Delta}$;*Rosa26*$^{ERT2\text{-}bsd/FlpRMCE\text{-}EV}$;*Pim1*$^{DR\text{-}GFP\text{-}hygro/wt}$ mES-cells using LentiCRISPRv2 vectors containing indicated sgRNAs. Cells were treated with 4-OHT to inactivate the *Brca1*^{Sco} allele and subsequently transfected with mCherry/I-SceI constructs. HR activity was determined by flow cytometry and was calculated as the percentage of GFP+ cells in the mCherry+ population relative to BRCA1 proficient parental cells. The experiment was performed three times and the data are plotted as mean with SEM. Statistics was performed by unpaired one-tailed students t-test (* = p-value <0.05; ** = p-value <0.01).

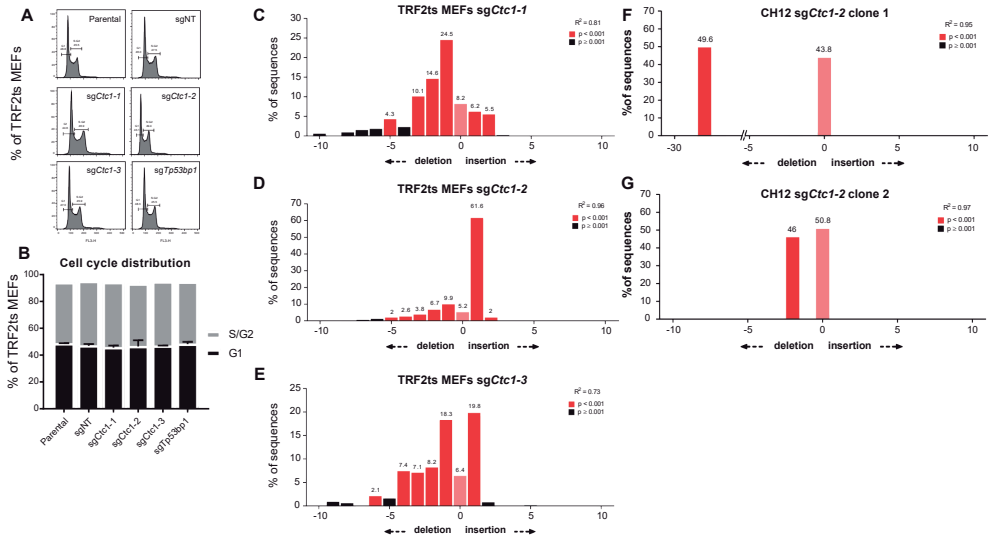

SUPPLEMENTARY FIGURE S4 | CTC1 facilitates cNHEJ at telomeric and non-telomeric DSBs. Related to Figure 5. *(A-B)* Cell cycle distribution profiles were determined by flow cytometry from TRF2ts MEFs transfected with pX330puro vectors containing indicated sgRNAs. The experiment was performed two times. *(C-E)* TIDE plots of TRF2ts MEFs targeted by indicated sgRNAs. *(F-G)* TIDE plots of the two CH12 clones that were successfully targeted with sg*Ctc1-2*.

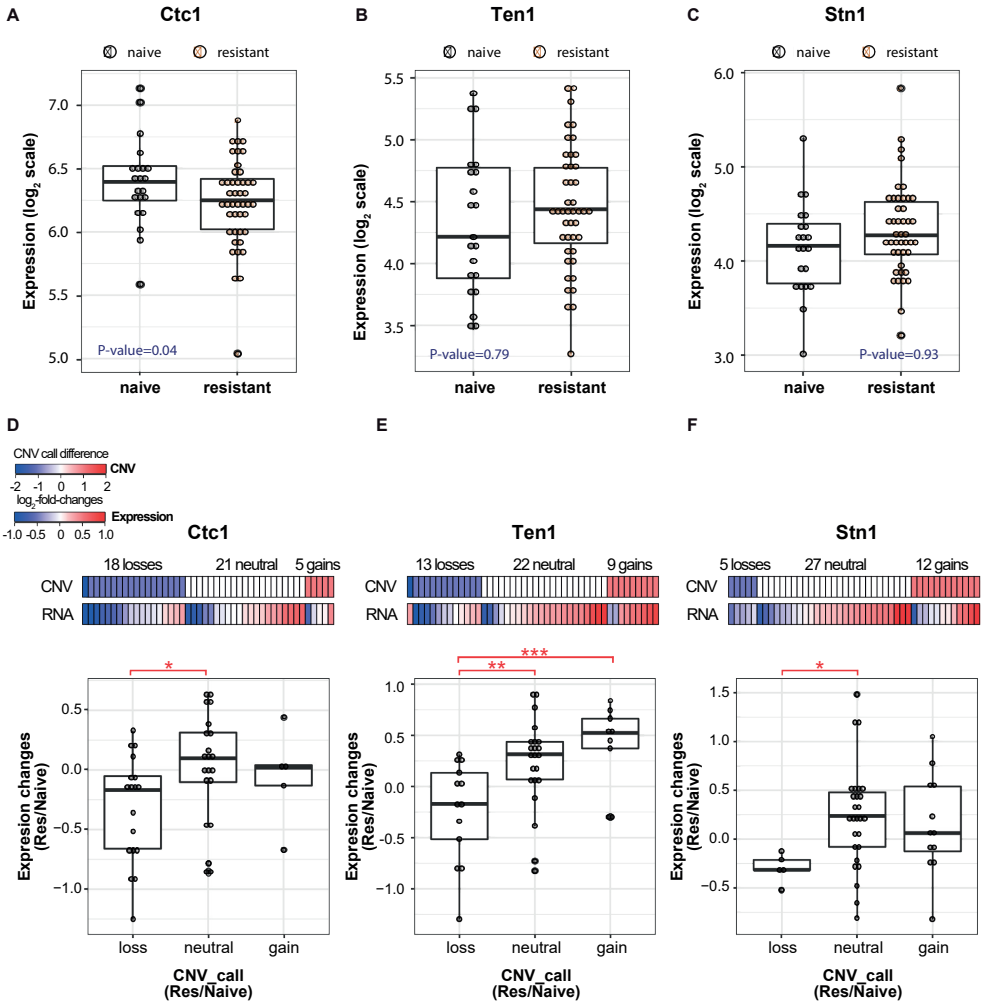

SUPPLEMENTARY FIGURE S5 | Expression and copy number profiles for CST complex genes (*Ctc1*, *Ten1*, and *Stn1*) in matched KB1P(M) naïve- and PARPi-resistant tumors for which both RNA-seq and CNV-seq were available. In total, 21 naïve and 44 resistant tumors from 21 donors were used in this analysis. Related to Figure 6. *(A-C)* mRNA expression levels (log2(CPM) of *Ctc1 (A)*, *Ten1 (B)*, and *Stn1 (C)*, between naïve and resistant tumors. P-values were obtained by one-tail t-test. *(D-F)* Correlation between mRNA levels and CNV for CST complex genes. CNV calling and gene expression levels of 44 resistant tumors were compared to those of corresponding naïve tumors. First heatmaps indicate copy number changes (red: copy number gain, blue: copy number loss) and second heatmaps indicate gene expression changes (red: upregulation, blue: downregulation) for the same tumors. Bottom boxplots indicate correlation between copy number changes and expression changes. Adjusted P-value were obtained by one-way anova and Tukey multiple pairwise-comparison. * Adj. P-value < 0.1, ** Adj. P-value < 0.05, *** Adj. P-value <0.01.

SUPPLEMENTARY TABLE S1 | Details of the Focused Mouse DDR Library, Related to Supplementary Materials and Methods can be accessed via the online version of this article.

SUPPLEMENTARY TABLE S2 | sgRNA and crRNA sequences. Related to Supplementary Materials and Methods.

Mouse gene name	Mouse sgRNA name	sgRNA sequence
Non-targeting	sgNT	TGATTGGGGGTCGTTCGCCA
Ctc1	sg*Ctc1-1*	CTTGAAGCCGAACAGTGCCA
Ctc1	sg*Ctc1-2*	CACGAGTTGCTCATACAAGG
Ctc1	sg*Ctc1-3*	CTGGTCGAATAACCCGCCTG
Stn1	sg*Stn1-1*	ATGATATCTACCCGCCTTAT
Stn1	sg*Stn1-2*	CAACGGGCATCCAATAAGGC
Ten1	sg*Ten1*	CTGCGAACATTTGGCAGGTA
Tp53BP1	sg*Tp53BP1*	GAACAATCTGCTGTAGAACA
Human gene name	**Human crRNA name**	**crRNA sequence**
Non-targeting	crNT-1	AAAACACGATGACGTCTCT
Non-targeting	crNT-2	AAACGAGAAGTTTGTACTA
CTC1	cr*CTC1-1*	TGCCAACTCAATCGCCGCC
CTC1	cr*CTC1-2*	TAGGCTGTACCAGGCCGAA
CTC1	cr*CTC1-3*	ACAGACCTATCGGCAGACT
TP53BP1	cr*TP53BP1-1*	TCTAGTGTGTTAGATCAGG
TP53BP1	cr*TP53BP1-2*	GGGGGTTTTCTAACTCCAC
TP53BP1	cr*TP53BP1-3*	GACTGCTAGGAACGATAAA

SUPPLEMENTARY TABLE S3 | PCR primer sequences. Related to Supplementary Materials and Methods.

sgRNA name	FW PCR primer	RV PCR primer	Source
sgNon-targeting	N.A.	N.A.	Duarte et al., 2017
sg*Ctc1-1*	TGTTCCAGACAGGGATTTTCCAA	AGGAGAGGGTTGCTTCAGGA	This paper
sg*Ctc1-2*	TGTTCCAGACAGGGATTTTCCAA	AGGAGAGGGTTGCTTCAGGA	This paper
sg*Ctc1-3*	ATTATGGTTAAGGGCGGGGGT	TGGCTACTGTTTCTCCACCAT	This paper
sg*Stn1-1*	GCATTTCAATTCTTCCACGGCT	CACTTGCCAAGGACTGACTC	This paper
sg*Stn1-2*	GCATTTCAATTCTTCCACGGCT	CACTTGCCAAGGACTGACTC	This paper
sg*Ten1*	GCCAGCTAGTCTTCCAAATGT	CAGCGTATGGTTCTCACTACC	This paper
sg*Tp53BP1*	TGAGAAATGGAGGCAACACCA	TGCAAATGTGGGCTACTGGG	This paper
Brca1-Sco allele	CACCTGCTCTGGCTGATG	AGGTCTGCCTGCCTCTACTTC	Bouwman et al., 2013
Brca1-DelSco allele	GTGGGCTTGTACTCGGTCAT	GCTGTTCTCCTCTTCCTCATC	Bouwman et al., 2013
iKRUNC sequencing primer	AAAGAATAGTAGACATAATAGC	N.A.	This paper

Supplementary References

1. Bouwman P, Aly A, Escandell JM, Pieterse M, Bartkova J, van der Gulden H, et al. 53BP1 loss rescues BRCA1 deficiency and is associated with triple-negative and BRCA-mutated breast cancers. Nat Struct Mol Biol. 2010; 17: 688-95.
2. Bouwman P, van der Gulden H, van der Heijden I, Drost R, Klijn CN, Prasetyanti P, et al. A high-throughput functional complementation assay for classification of BRCA1 missense variants. Cancer Discov. 2013; 3: 1142-55.
3. Peuscher MH, Jacobs JJ. DNA-damage response and repair activities at uncapped telomeres depend on RNF8. Nat Cell Biol. 2011; 13: 1139-45.
4. Follenzi A, Ailles LE, Bakovic S, Geuna M, Naldini L. Gene transfer by lentiviral vectors is limited by nuclear translocation and rescued by HIV-1 pol sequences. Nat Genet. 2000; 25: 217-22.
5. Duarte AA, Gogola E, Sachs N, Barazas M, Annunziato S, J RdR, et al. BRCA-deficient mouse mammary tumor organoids to study cancer-drug resistance. Nat Methods. 2018; 15: 134-40.
6. Koo BK, Stange DE, Sato T, Karthaus W, Farin HF, Huch M, et al. Controlled gene expression in primary Lgr5 organoid cultures. Nat Methods. 2011; 9: 81-3.
7. Prahallad A, Heynen GJ, Germano G, Willems SM, Evers B, Vecchione L, et al. PTPN11 Is a Central Node in Intrinsic and Acquired Resistance to Targeted Cancer Drugs. Cell Rep. 2015; 12: 1978-85.
8. Cong L, Ran FA, Cox D, Lin S, Barretto R, Habib N, et al. Multiplex genome engineering using CRISPR/Cas systems. Science. 2013; 339: 819-23.
9. Harmsen T, Klaasen S, van de Vrugt H, Te Riele H. DNA mismatch repair and oligonucleotide end-protection promote base-pair substitution distal from a CRISPR/Cas9-induced DNA break. Nucleic Acids Res. 2018; 46: 2945-55.
10. Jaspers JE, Kersbergen A, Boon U, Sol W, van Deemter L, Zander SA, et al. Loss of 53BP1 causes PARP inhibitor resistance in Brca1-mutated mouse mammary tumors. Cancer Discov. 2013; 3: 68-81.
11. Costantino L, Sotiriou SK, Rantala JK, Magin S, Mladenov E, Helleday T, et al. Break-induced replication repair of damaged forks induces genomic duplications in human cells. Science. 2014; 343: 88-91.
12. Xu G, Chapman JR, Brandsma I, Yuan J, Mistrik M, Bouwman P, et al. REV7 counteracts DNA double-strand break resection and affects PARP inhibition. Nature. 2015; 521: 541-4.
13. Oplustil O'Connor L, Rulten SL, Cranston AN, Odedra R, Brown H, Jaspers JE, et al. The PARP Inhibitor AZD2461 Provides Insights into the Role of PARP3 Inhibition for Both Synthetic Lethality and Tolerability with Chemotherapy in Preclinical Models. Cancer research. 2016; 76: 6084-94.
14. Robinson MD, McCarthy DJ, Smyth GK. edgeR: a Bioconductor package for differential expression analysis of digital gene expression data. Bioinformatics. 2010; 26: 139-40.
15. Liu X, Holstege H, van der Gulden H, Treur-Mulder M, Zevenhoven J, Velds A, et al. Somatic loss of BRCA1 and p53 in mice induces mammary tumors with features of human BRCA1-mutated basal-like breast cancer. Proc Natl Acad Sci U S A. 2007; 104: 12111-6.
16. Koike-Yusa H, Li Y, Tan EP, Velasco-Herrera Mdel C, Yusa K. Genome-wide recessive genetic screening in mammalian cells with a lentiviral CRISPR-guide RNA library. Nat Biotechnol. 2014; 32: 267-73.
17. Elstrodt F, Hollestelle A, Nagel JH, Gorin M, Wasielewski M, van den Ouweland A, et al. BRCA1 mutation analysis of 41 human breast cancer cell lines reveals three new deleterious mutants. Cancer research. 2006; 66: 41-5.
18. Tzelepis K, Koike-Yusa H, De Braekeleer E, Li Y, Metzakopian E, Dovey OM, et al. A CRISPR Dropout Screen Identifies Genetic Vulnerabilities and Therapeutic Targets in Acute Myeloid Leukemia. Cell Rep. 2016; 17: 1193-205.
19. Wang G, Zimmermann M, Mascall K, Lenoir WF, Moffat J, Angers S, et al. Identifying drug-gene interactions from CRISPR knockout screens with drugZ. bioRxiv. 2017: 232736.
20. de Jager M, Dronkert ML, Modesti M, Beerens CE, Kanaar R, van Gent DC. DNA-binding and strand-annealing activities of human Mre11: implications for its roles in DNA double-strand break repair pathways. Nucleic Acids Res. 2001; 29: 1317-25.
21. Boersma V, Moatti N, Segura-Bayona S, Peuscher MH, van der Torre J, Wevers BA, et al. MAD2L2 controls DNA repair at telomeres and DNA breaks by inhibiting 5' end resection. Nature. 2015; 521: 537-40.

22. Gogola E, Duarte AA, de Ruiter JR, Wiegant WW, Schmid JA, de Bruijn R, et al. Selective Loss of PARG Restores PARylation and Counteracts PARP Inhibitor-Mediated Synthetic Lethality. Cancer cell. 2018; 33: 1078-93.e12.
23. Dobin A, Davis CA, Schlesinger F, Drenkow J, Zaleski C, Jha S, et al. STAR: ultrafast universal RNA-seq aligner. Bioinformatics. 2013; 29: 15-21.
24. Ewels P, Magnusson M, Lundin S, Käller M. MultiQC: summarize analysis results for multiple tools and samples in a single report. Bioinformatics. 2016; 32: 3047-8.
25. Liao Y, Smyth GK, Shi W. featureCounts: an efficient general purpose program for assigning sequence reads to genomic features. Bioinformatics. 2014; 30: 923-30.
26. Li H, Durbin R. Fast and accurate long-read alignment with Burrows-Wheeler transform. Bioinformatics. 2010; 26: 589-95.
27. Scheinin I, Sie D, Bengtsson H, van de Wiel MA, Olshen AB, van Thuijl HF, et al. DNA copy number analysis of fresh and formalin-fixed specimens by shallow whole-genome sequencing with identification and exclusion of problematic regions in the genome assembly. Genome Res. 2014; 24: 2022-32.